microbial cell

Research Article

www.microbialcell.com

Integrative Omics reveals changes in the cellular landscape of peroxisome-deficient *pex3* yeast cells

Tjasa Kosir[1,a], Hirak Das[2,a], Marc Pilegaard Pedersen[1], Ann-Kathrin Richard[2], Marco Anteghini[3,4], Vitor Martins dos Santos[4,5], Silke Oeljeklaus[2], Ida J. van der Klei[1,*] and Bettina Warscheid[2,*]

[1] Molecular Cell Biology, Groningen Biomolecular Sciences and Biotechnology Institute (GBB) University of Groningen, PO Box 11103, 9300 CC Groningen, The Netherlands. [2] Theodor-Boveri-Institute, Biochemistry II, Faculty of Chemistry and Pharmacy, University of Würzburg, 97074 Würzburg, Germany. [3] Laboratory of Systems and Synthetic Biology, Wageningen University & Research, Wageningen WE, The Netherlands. [4] Lifeglimmer GmbH, Berlin, Germany. [5] Department of Bioprocess Engineering, Wageningen University & Research, Wageningen WE, The Netherlands.

* Corresponding Authors:
Bettina Warscheid, Theodor-Boveri-Institute, Biochemistry II, Faculty of Chemistry and Pharmacy, University of Würzburg, 97074 Würzburg, Germany; E-mail: bettina.warscheid@uni-wuerzburg.de
Ida J. van der Klei, Molecular Cell Biology, Groningen Biomolecular Sciences and Biotechnology Institute (GBB) University of Groningen, PO Box 11103, 9300 CC Groningen, The Netherlands; E-mail: i.j.van.der.klei@rug.nl

[a] Equal contribution as first authors.

ABSTRACT Peroxisomes are organelles that are crucial for cellular metabolism, but they also play important roles in non-metabolic processes such as signalling, stress response or antiviral defense. To uncover the consequences of peroxisome deficiency, we compared *Saccharomyces cerevisiae* wild-type with *pex3* cells, which lack peroxisomes, employing quantitative proteomics and transcriptomics technologies. Cells were grown on acetate, a carbon source that requires peroxisomal enzymes of the glyoxylate cycle to generate energy and essential carbohydrates, and that does not repress the expression of peroxisomal genes. Our integrative omics analysis reveals that the absence of peroxisomes induces distinct responses at the level of the transcriptome and proteome. Transcripts of genes and corresponding proteins that are associated with peroxisomal β-oxidation were mostly increased in *pex3* cells. In contrast, levels of peroxins were regulated at protein but not at transcript level. Membrane-bound peroxins were reduced, whereas the soluble receptors Pex5 and Pex7 were increased in abundance in *pex3* cells. Interestingly, we found several non-peroxisomal transcript and proteins regulated in *pex3* cells including mitochondrial proteins involved in respiration or import processes, which led to the identification of the mitochondrial pyruvate carrier Mpc1/3 as so far unnoticed transporter present in the peroxisomal membrane. Our results reveal the impact of the absence of peroxisomes in pex3 yeast cells and represent a rich resource of genes/proteins for follow-up studies to obtain a deeper understanding of peroxisome biology in a cellular context.

doi: 10.15698/mic2025.02.842
Received originally: 08.05.2024;
in revised form: 28.11.2024,
Accepted 05.12.2024,
Published 20.02.2025.

Keywords: peroxisome, yeast, proteome, transcriptome, *PEX* genes, β-oxidation, mitochondria.

Abbreviations:
ERAD – endoplasmic reticulum unfolded protein response,
FM – fluorescence microscopy,
FP – fluorescence protein,
IMM – Inner mitochondrial membrane,
PMP – peroxisomal membrane protein,
PTS – peroxisomal targeting signal,
WT – wild type.

INTRODUCTION

Peroxisomes are organelles that occur in almost all eukaryotic cells. Their importance is illustrated by pathogenic mutations that can cause devastating peroxisomal diseases such as Zellweger spectrum disorders [1]. They consist of a proteinaceous matrix that contains enzymes involved in various metabolic pathways and is bound by a single membrane. Common peroxisomal enzymes are hydrogen peroxide-producing oxidases, catalase for detoxification of the hydrogen peroxide, and enzymes of the β-oxidation

pathway. Depending on the organism, developmental stage and cell type, peroxisomes can further harbour enzymes involved in a broad spectrum of other metabolic pathways such as penicillin biosynthesis in filamentous fungi, ether lipid biosynthesis in mammals or photorespiration in plant (reviewed in [2-5]). The peroxisomal membrane contains a highly diverse set of proteins including membrane bound peroxins (encoded by *PEX* genes), which are required for the biogenesis of the organelle [6], solute transporters, and proteins involved in organelle fission and inheritance (reviewed in [6-8]). Peroxisomes also fulfil crucial non-metabolic functions. For instance, mammalian peroxisomes can serve as intracellular signalling platforms in innate immunity and inflammation [9]. In addition, they are implicated in ageing [10] and in antiviral response [11]. Hence, a detailed understanding of the molecular mechanisms involved in peroxisome biology is important for human health and disease.

Yeasts are simple model organisms that are extensively used to study peroxisomes. Since the molecular mechanisms of many processes in peroxisome biology are conserved, the knowledge obtained by yeast peroxisome research can be translated to higher eukaryotes, including humans. Yeast research substantially contributed to the identification and characterization of peroxins [12-14]. Mutant screens were performed to isolate strains defective in various aspects of peroxisome biology. The analysis of yeast libraries by high throughput fluorescence microscopy (FM) and proteomics studies of isolated peroxisomes or affinity-purified protein complexes of peroxisomal proteins, mostly peroxins, resulted in the discovery of many additional proteins and processes related to peroxisome biology [15-19].

Peroxisomes cannot function in isolation but must communicate and cooperate with their environment to exchange metabolites and coordinate cellular responses [20]. For instance, in yeast, β-oxidation of fatty acids is confined to peroxisomes and results in the formation of acetyl-CoA, which is transferred to mitochondria for further oxidation via the citric acid cycle. Recent studies indicate that physical contacts between both organelles stimulate acetyl-CoA transfer between both organelles [21]. Moreover, the small GTPase Arf1 was demonstrated to localize to these contacts, where it coordinates acetyl-CoA transfer [22]. Importantly, peroxisomes also form physical contacts with other cell organelles, but the function of most of them is relatively unexplored [23]. In sum, further research is needed to better understand how peroxisomes communicate and cooperate with their environment and what are the consequences of the loss of peroxisomes in a cellular context.

In this work, we utilized *Saccharomyces cerevisiae* yeast lacking Pex3 (*pex3* cells) as a model system to study changes in the proteome and transcriptome in consequence of the loss of peroxisomes. Pex3 is a peroxisomal membrane protein (PMP) required for the insertion of further PMPs into the peroxisomal membrane, including proteins of the peroxisomal matrix protein import machinery, and, thus, Pex3 is indispensable for peroxisome biogenesis [24-26]. We previously showed that *pex3* cells harbour small membrane vesicles that contain a subset of PMPs, but peroxisomal matrix proteins are generally absent from these vesicles [27]. Since peroxisomes are the only site of fatty acid β-oxidation in yeast, *pex3* cells do not grow when oleic acid is provided as sole carbon source [25]. However, *pex3* cells are fully viable and capable of growing on several other carbon sources. For our study, we chose acetate as sole carbon source. Acetate metabolism requires activation to acetyl-CoA followed by the reactions of the glyoxylate cycle, a metabolic pathway that is present in yeast and plants [28, 29]. The glyoxylate cycle then provides metabolites for the production of essential carbohydrates through gluconeogenesis and ATP via the tricarboxylic acid cycle and oxidative phosphorylation [28, 30]. Cells lacking any of the glyoxylate cycle enzymes (except for Cit2) do not grow on acetate-containing medium [31], which demonstrates the importance of this pathway. Notably, we refrained from growing yeast cells on glucose because it represses the expression of many peroxisomal genes [32].

In this study, we show that peroxisome deficiency elicits specific responses at the transcriptome and proteome level in *pex3* cells. While the levels of most peroxisomal β-oxidation enzymes and the soluble receptor proteins Pex5 and Pex7 were increased, virtually all membrane bound peroxins were reduced in abundance in *pex3* cells. Importantly, we found numerous non-peroxisomal proteins to be regulated in *pex3* cells, which led to the finding that a fraction of the mitochondrial pyruvate carriers Mpc1/3 localize to peroxisomal membranes. Interestingly, the abundance of a set of mitochondrial proteins involved in protein import, refolding and mitochondrial respiration was increased in *pex3* cells, indicating that loss of peroxisomes affects also non-peroxisomal processes. We summarized our quantitative data in a compartment-specific cellular map, which provides a rich source for selecting candidates for further studies to potentially reveal other so far unknown new peroxisomal proteins and the processes affected by peroxisome deficiency.

RESULTS

Acetate is a suitable carbon source for comparative quantitative omics studies of WT and *pex3* cells

We first evaluated if acetate is an appropriate carbon source to study the effects of peroxisome deficiency in *pex3* cells on the cellular proteome and transcriptome. To this end, we studied the localization of selected enzymes involved in acetate metabolism via the glyoxylate cycle (i.e., the citrate synthase Cit2, the malate dehydrogenase

Mdh3, and the carnitine acetyl-CoA transferase Cat2) in acetate grown wild type (WT) cells. Cit2, Mdh3 and Cat2 localize to peroxisomes when cells are grown on oleate (reviewed in [30, 33-36]). Both Cit2 and Mdh3 have a C-terminal peroxisomal targeting signal of type 1 (PTS1), which targets them to the peroxisomal matrix via the Pex5-dependent PTS1 import pathway ([26] and references therein). Cat2 has a dual localization in mitochondria and peroxisomes [37] and, thus, contains both a C-terminal PTS1 and an N-terminal mitochondrial targeting signal [38]. All three proteins were tagged at the N- or C-terminus with a fluorescence protein (FP), and their subcellular localization was analyzed by FM using a strain producing Pex14-mKate2 as a peroxisome marker. As shown in **Figure 1a**, cells expressing the N-terminally tagged proteins all showed a punctate pattern co-localizing with Pex14-mKate2, indicative of a peroxisomal localization. Since the N-terminal tag masks the mitochondrial targeting signal in Cat2, a mitochondrial localization of Cat2 was not observed. The punctate pattern of all three proteins was lost when proteins were expressed in *pex3* cells, which lack peroxisomes (**Figure 1b**; see Figures S1a and S1b for validation of the *pex3* strain). The punctate pattern was also lost when the FP was fused to the C-terminus of Mdh3 or Cit2. These cells showed a diffuse cytosolic fluorescence pointing to an impaired import of these proteins into the peroxisomal matrix resulting from the FP tag masking the PTS1 (**Figure 1c**). C-terminally tagged Cat2 localized to mitochondria as is evident from mitotracker staining (**Figure 1d**). This is in line with earlier data which show that when the PTS1 of Cat2 is masked, the protein is routed to mitochondria via the N-terminal mitochondrial presequence. Taken together, our FM data confirm a peroxisomal localization for Cit2, Mdh3, and Cat2 in acetate grown WT yeast cells.

For a reliable comparison of the proteome and transcriptome of WT and *pex3* cells, it is essential that cells grow identically to avoid artifacts caused by differences in growth parameters. As shown in **Figure 1e**, *pex3* cells showed WT-like growth in acetate-containing medium. Moreover, measurements of the residual concentrations of acetate in the growth medium revealed that acetate consumption was the same in both strains (**Figure 1f**). Thus, we concluded that the loss of peroxisomes in *pex3* cells neither affects the growth on acetate nor the acetate consumption. Moreover, our data show that peroxisomes are involved in acetate metabolism since WT cells harbor several enzymes required for this process. This makes acetate a suitable carbon source for comparative quantitative omics studies of WT and *pex3* cells.

Quantitative proteome and transcriptome analysis of WT versus *pex3* cells

To globally study the loss of peroxisomes in *S. cerevisiae* *pex3* cells for its effect on the cellular proteome and transcriptome, WT and *pex3* cells were grown in batch cultures using acetate as a carbon source and harvested in the early exponential growth phase. Whole cell proteome and transcriptome analyses were performed from the identical samples, followed by quantitative data analysis and integrative evaluation of the obtained omics data (**Figure 2a**).

For quantitative whole cell proteomics of WT and *pex3* cells, we employed peptide stable isotope dimethyl labeling [43], orthogonal peptide separation by high and low pH reversed-phase liquid chromatography (LC) followed by high-resolution mass spectrometry (MS). This in-depth analysis resulted in the quantification of 3,921 protein groups in at least two out of three replicates, of which 3,700 (94.4%) were quantified in all three replicates (Table S1a). We found 79 proteins with an average change in abundance of at least 1.5-fold (34/45 proteins reduced/increased; p-value of < 0.05, n=3) (**Figure 2b**, Table S1a). Using this proteomics approach, we quantified 92 peroxisomal proteins, with 17/11 reduced/increased in abundance (p-value < 0.05). Furthermore, most PMPs (10 out of 12, p-value < 0.05) were more than 1.5-fold reduced in abundance, whereas a few soluble peroxisomal proteins (5 out of 16, p-value < 0.05) were more than 1.5-fold increased in *pex3* cells (**Figure 2b** and Table S1a). Quantitative Western blotting of selected regulated proteins confirmed abundance changes in *pex3* cells determined by quantitative MS analysis as shown for the soluble peroxisomal protein Pot1 and the PTS1 receptor protein Pex5, which were both increased in *pex3* cells, and the PMP Pex14, which was 1.9-fold decreased. In addition, a 2.5-fold increase in abundance of the plasma membrane and vacuole transporter Tpo4 in *pex3* cells was confirmed by Western blotting (Figures S2a and S2b). Western blot analyses of protein levels in *pex3* cells transformed with a plasmid for expression of the *PEX3* gene (pPEX3; [44]) revealed that the levels of selected proteins were restored to virtually WT levels after reintroduction of *PEX3* (Figure S2c), which demonstrates that the effects we observe in *pex3* cells are Pex3-specific.

The complementary analysis of the transcriptome of WT and *pex3* cells resulted in the identification of 5,460 transcripts with at least 10 reads on average across all samples and it includes 123 peroxisomal transcripts (Tables S1b). For 3,952 transcripts, the respective proteins were also quantified by proteomics analysis (Figure S2d, Table S1c). In addition to the 91 peroxisomal transcripts/proteins detected by both methods, we found additional 32 peroxisomal transcripts which were not covered by whole cell proteomics. These include low abundance peroxisomal proteins such as the PTS2 co-receptors Pex18 and Pex21, the alternative PTS1 receptor Pex9, or the RING finger proteins Pex2 and Pex10 (Table

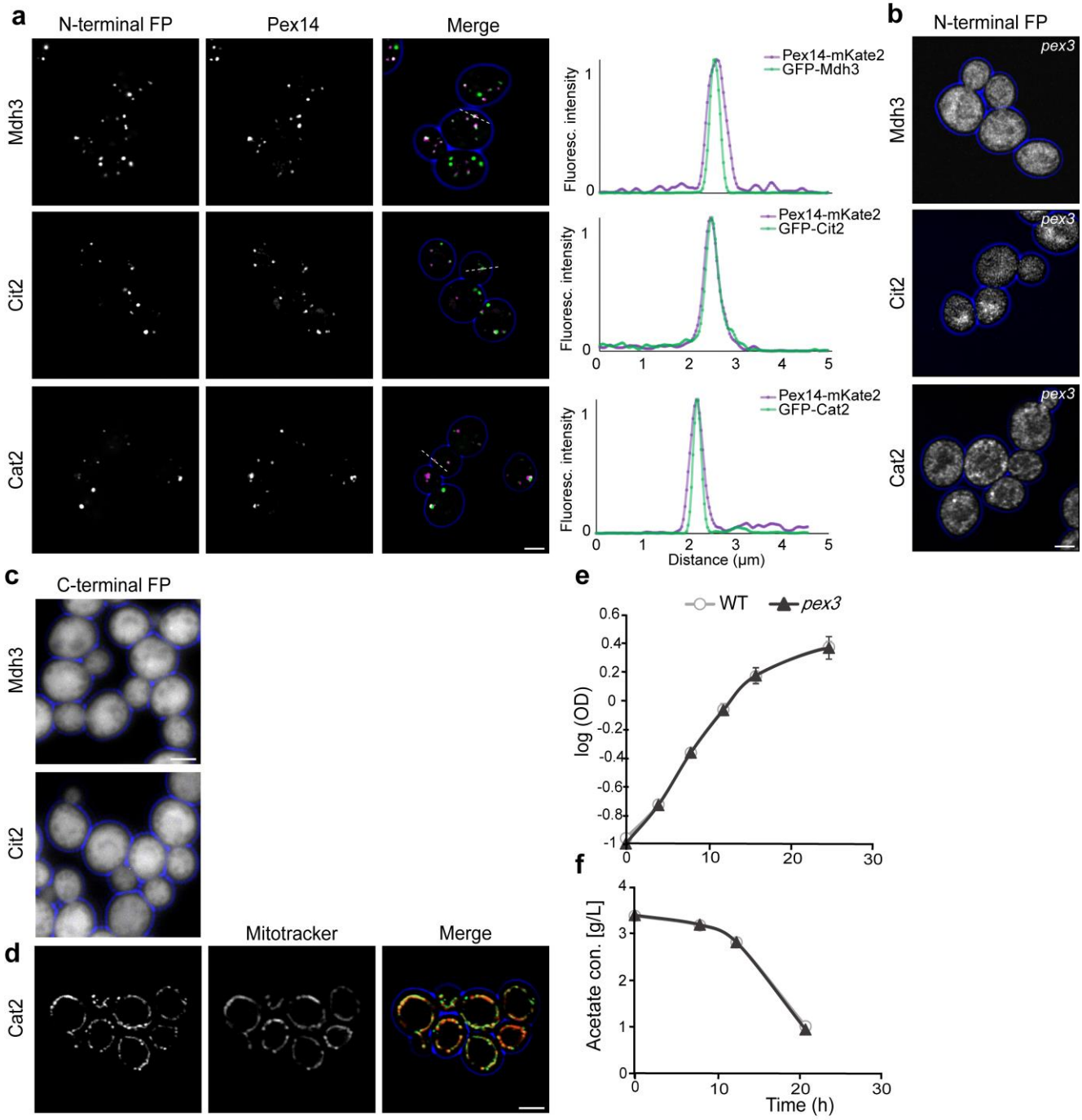

FIGURE 1 ● Validation of acetate as a suitable carbon source for the omics comparison of WT and *pex3* cells. **(a)** Airyscan fluorescence microscopy analysis of acetate grown cells expressing Mdh3, Cit2 or Cat2 with the fluorescent protein (FP) GFP at the N-terminus under control of the *NOP1* promoter. Pex14-mCherry was used as a peroxisomal marker. The cell contour is shown in blue. Scale bar: 2.5 µm. Graphs show normalized fluorescence intensity along the lines indicated in the merged images. **(b)** Airyscan fluorecence microscopy images of acetate grown *pex3* cells producing the indicated proteins . The cell contour is shown in blue. Scale bar: 2.5 µm. **(c)** FM analysis of acetate grown cells tagged with the FP NeonGreen (Mdh3) or GFP (Cit2) at the C-terminus under control of the endogenous promoter. The cell contour is shown in blue. Scale bar: 2.5 µm. **(d)** Airyscan fluorescenc microscopy of acetate grown cells expressing Cat2-NeonGreen under the endogenous promoter. Mitochondria are marked by MitoTracker Red. The cell contour is shown in blue. Scale bar: 2.5 µm. **(e)** Growth curves of WT and *pex3* cells grown in batch cultures on acetate medium. The cell density is indicated as log optical density (OD) at 660 nm. The error bars represent the standard deviation (SD) from three independent experiments. **(f)** Acetate concentrations (g/L) in the media of WT and *pex3* cultures. The error bars represent SD from three independent experiments. Error bars are smaller than the symbols.

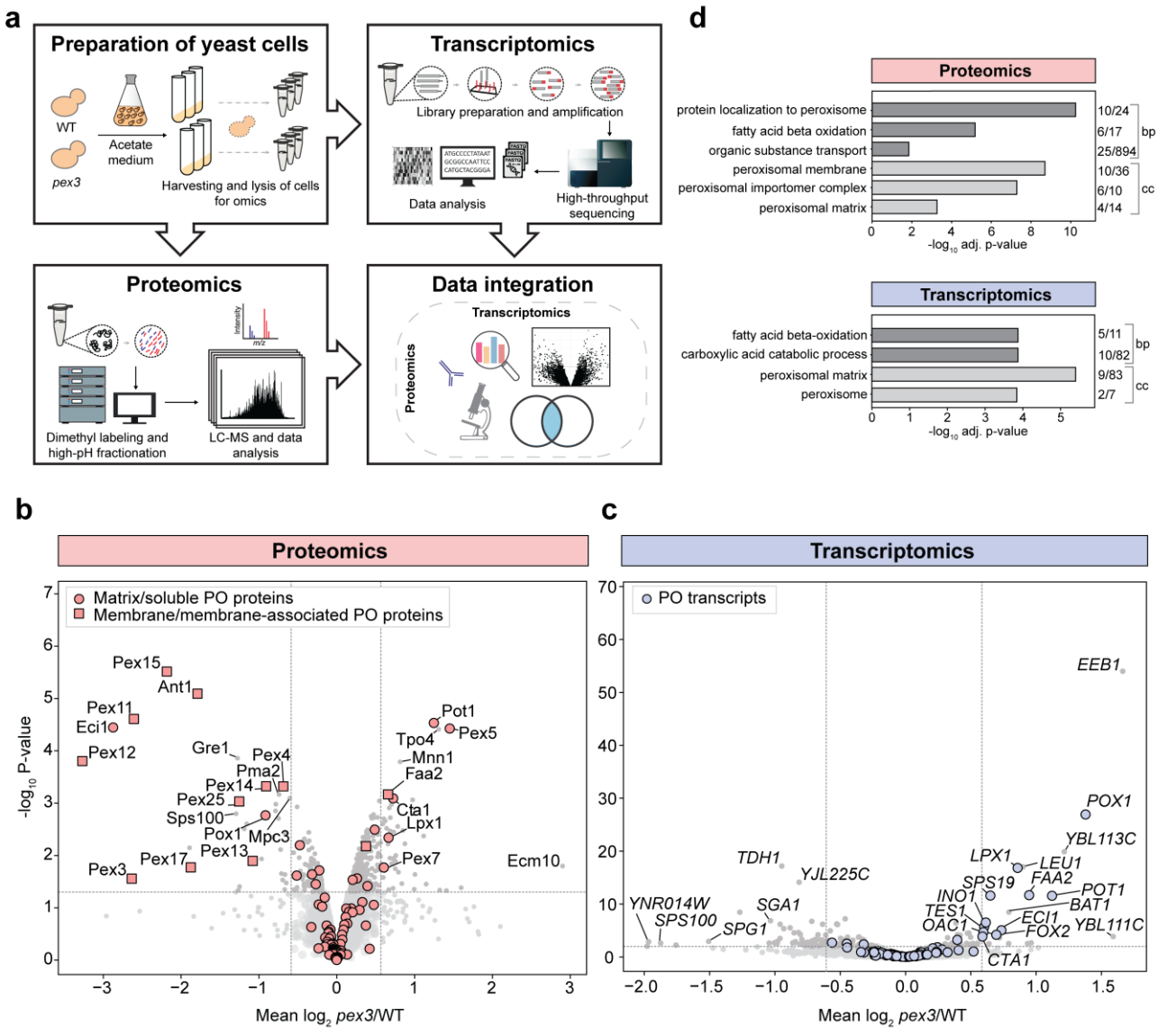

FIGURE 2 **Proteomics and transcriptomics analysis of *S. cerevisiae* WT and *pex3* cells. (a)** Outline of the experimental strategy employed for the systematic analysis of global changes in the proteome and transcriptome caused by the absence of peroxisomes in *pex3* cells. Experiments were performed in three independent biological replicates, and the same samples were analyzed by quantitative proteomics and transcriptomics. **(b, c)** Global differences in protein **(b)** and transcript **(c)** levels in *pex3 versus* WT cells. Mean $\log_2$ *pex3*/WT ratios were plotted against the corresponding log-transformed p-value ($-\log_{10}$) determined using the 'linear models for microarray data' (limma) approach (two-sided t-test; n=3) for the proteomics and the Wald test for the transcriptomics data. Note that Pex3 was in fact absent in the *PEX3* deletion strain. The ratio we report is based on a feature of the data analysis software. See section "MS data analysis" in Materials and methods for a more detailed explanation. Horizontal and vertical lines indicate a p-value of 0.05 and a fold-change of ≤ 0.66 or ≥ 1.5, respectively. Information about a peroxisomal localization of proteins or association with peroxisomes is based on [15, 16, 39-42]. PO, peroxisomal and peroxisome-associated proteins or transcripts. **(d)** GO term overrepresentation analysis of proteins and transcripts with a fold-change of ≤ 0.66 or ≥ 1.5 (p-value < 0.05) for the domains "biological process" (bp) and "cellular component" (cc). Listed are selected terms with an adjusted (adj.) p-value of < 0.05. Numbers indicate the number of proteins or transcripts assigned to a given term and the number of proteins/transcripts with this term in the proteomics or transcriptomics dataset.

S1c). Overall, 102 transcripts were regulated by a factor of at least 1.5-fold (25/77 transcripts increased/reduced; p-value < 0.05, n=3) in *pex3* cells. Remarkably, *PEX3* deletion significantly affected only five soluble peroxisomal proteins at the transcript level, which were all upregulated in *pex3* cells (Figure 2c). As shown for protein levels (Figure S2c), the levels of selected transcripts with changed abundance in *pex3* cells reached WT-like expression levels after reintroduction of *PEX3* (Figure S2e).To obtain a first overview of the main processes affected by the loss of peroxisomes in acetate grown *S. cerevisiae* cells, we performed Gene Ontology (GO) term overrepresentation analysis for the domains "Biological Process" and "Cellular Component" for regulated proteins and transcripts with a minimum fold-change of ±1.5 and a p-value < 0.05. The analysis shows that loss of Pex3 affects proteins that are linked to "protein localization to peroxisome", "fatty acid beta-oxidation", and, more general, "organic substance transport" and are present in the "peroxisomal membrane" including the "peroxisomal importomer complex" and the

"peroxisomal matrix", whereas regulated transcripts are mainly associated with the "peroxisomal matrix" and "fatty acid beta-oxidation" (**Figure 2d**, Table S2).

Taken together, our proteomics data reveal that the loss of peroxisomes largely affects peroxisomal matrix enzymes of the β-oxidation pathway and proteins of the peroxisomal membrane. Consistent with these data, transcripts of peroxisomal β-oxidation enzymes were upregulated, whereas only non-peroxisomal transcripts were found to be downregulated in *pex3* cells. Furthermore, the regulation of numerous non-peroxisomal proteins and transcripts in *pex3* cells indicates that the elicited cellular responses go beyond peroxisomes.

Functional classification of regulated peroxisomal proteins and transcripts in *pex3* cells

To examine the changes in *pex3* cells in detail, we classified peroxisomal proteins into different functional groups: (1) peroxisomal biogenesis factors (peroxins, *PEX* genes), (2) β-oxidation enzymes and other peroxisomal matrix proteins, (3) proteins with a function in the glyoxylate cycle, and (4) solute transporters. In our analysis of proteomics and transcriptomics data displayed in volcano plots, we also directly compared changes in the proteome and transcriptome in consequence of *PEX3* deletion. To this end, the mean log2 *pex3*/WT ratios of transcripts and proteins were plotted against each other.

Changes in the levels of peroxins are independent of transcription. Peroxisomal proteins involved in the biogenesis of peroxisomes (peroxins, *PEX* genes) are of crucial importance for peroxisomal functions, and in *S. cerevisiae*, 29 peroxins have been identified so far [6]. In total, we quantified 19 peroxins at the protein level and all *PEX* transcripts except for *PEX3*. We found that membrane-localized peroxins, which play a role in peroxisomal matrix protein import, are considerably decreased in abundance at the whole cell level (**Figure 3a**). Exceptions are Pex8, which is attached to the luminal side of the peroxisomal membrane [45], and Pex22. The members of the Pex30 family, Pex29, Pex30, and Pex31, which do not reside in the peroxisomal membrane, but in the cortical ER membrane [17,18] were also unchanged. The opposite regulation was found for the cytosolic receptor proteins Pex5 and Pex7, which are essential for the import of PTS1- and PTS2-containing proteins, respectively. The finding was most pronounced for the PTS1 receptor Pex5, with a 2.7-fold increase in abundance.

The AAA-proteins Pex1 and Pex6 are essential for the peroxisomal export of the Pex5 to the cytosol [46]. Interestingly, both peroxins were not altered in abundance, although levels of their peroxisomal membrane anchor Pex15 were strongly reduced. This is likely related to the fact that Pex1 and Pex6 can form a stable, soluble hexameric complex in the absence of Pex15 [47]. We observed an opposite regulation for Pex4, which is involved in Pex5 ubiquitination after the translocation of cargo proteins into the peroxisomal matrix [48, 49]. Whereas levels of its membrane anchor Pex22 remained unchanged, Pex4 abundance was considerably decreased in the absence of Pex3 (**Figure 3a**).

In *S. cerevisiae*, Pex3 and Pex19 have been identified as necessary for PMP targeting [24]. In the absence of Pex3, we found that the cytosolic PMP receptor/chaperone Pex19 was only slightly increased in abundance, whereas levels of Pex19 cargo PMPs were reduced, including peroxins involved in (i) the import of peroxisomal matrix proteins [Pex14, Pex13, Pex17 (docking complex), Pex12 (RING complex), and Pex15 (export complex)], and (ii) peroxisome proliferation (Pex11 and Pex25). In stark contrast to these proteome data, transcriptomics analysis revealed that none of the *PEX* transcripts were regulated in *pex3* cells (**Figure 3a**, Table S1d).

Other proteins that are relevant in peroxisome biology, such as proteins that play a role in organelle fission (Dnm1, Vps1), inheritance (Inp1, Inp2) or pexophagy (Atg36) were all unchanged at the protein and transcript level (Table S1d).

To conclude, our omics data indicate that *PEX3* deletion results in unbalanced levels of peroxins involved in the late steps of peroxisomal matrix protein import, which involves the recycling of the peroxisomal receptor proteins Pex5 and Pex7. Both cytosolic receptor proteins accumulate in the absence of Pex3, which might result from the reduction in the ubiquitination factors Pex4 and Pex12. Since transcript levels remained unaltered in *pex3* cells, the observed changes in peroxin abundances are governed by posttranscriptional mechanisms, with membrane-localized peroxins presumably degraded in the absence of the target membrane.

Central β-oxidation enzymes are upregulated in the absence of Pex3. We asked whether the increased abundance of the PTS1 and PTS2 receptor proteins is accompanied by increased levels of peroxisomal matrix proteins. To address this, we examined changes in protein and transcript levels of peroxisomal enzymes in *pex3* compared to WT cells. Remarkably, β-oxidation enzymes (i.e., Fox2, Pot1, Faa2) were consistently upregulated at protein and transcript level (**Figure 3b**; Table S1d), with a few exceptions: first, auxiliary β-oxidation enzymes (Tes1, Sps19) and peroxisomal isocitrate dehydrogenase (Idp3) that is required for β-oxidation were mildly affected only at transcript level, and second, Pox1 and Eci1 were markedly decreased at protein but increased at transcript level. A recent study revealed that the protein levels of Pox1 are posttranslationally regulated by Arf1 {22]. Although yeast cells were grown under different conditions in this study, the same process may possibly also be responsible for the low Pox1 levels in *pex3* cells.

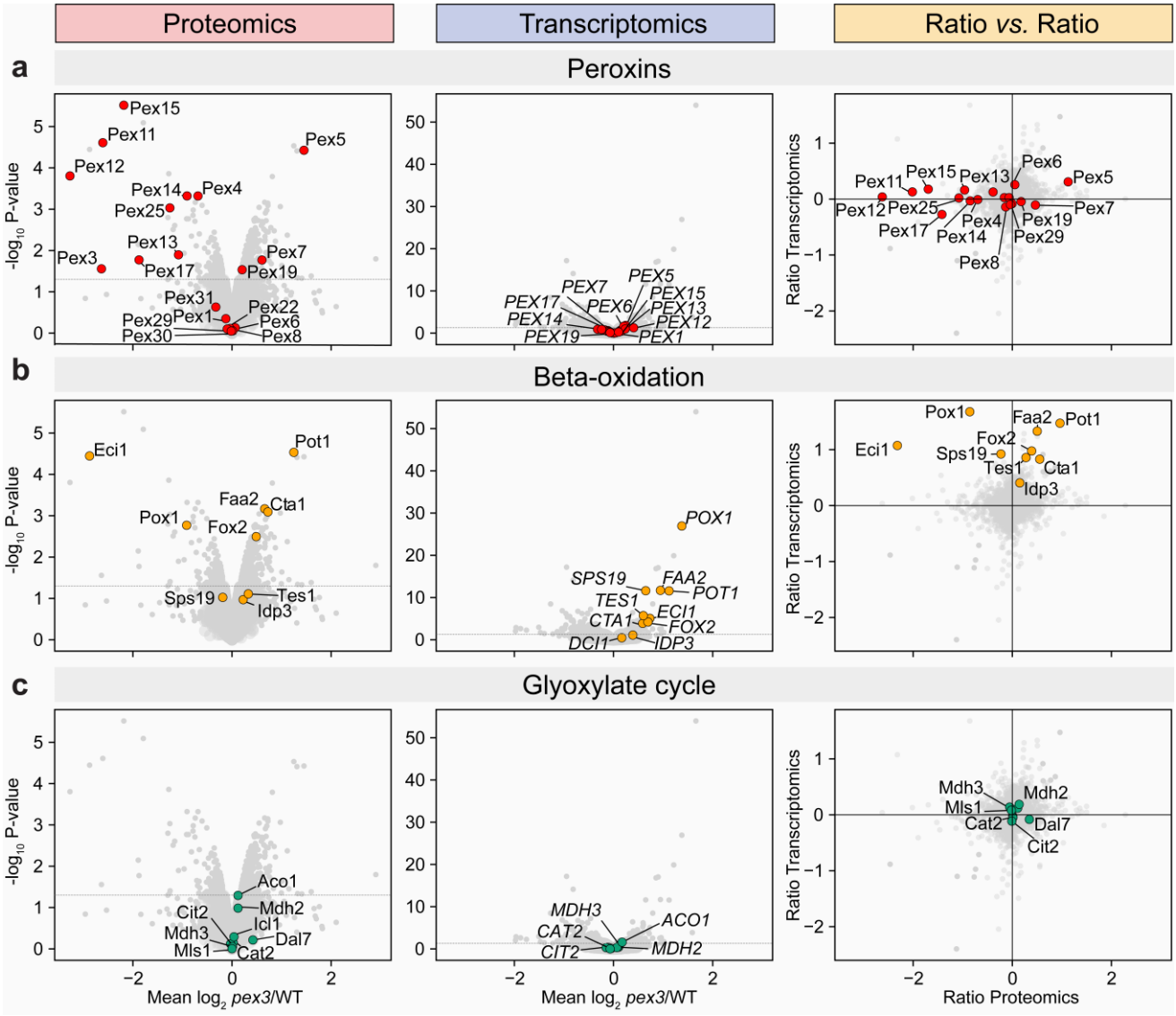

FIGURE 3 ● **Effect of the loss of Pex3 on the levels of proteins and transcripts associated with peroxisomal processes.** Same volcano plots as in Figures 2b and 2c depicting the results of the quantitative proteomics (left) and transcriptomics (middle) analyses and ratio-*versus*-ratio plots of both omics data (right) highlighting all peroxins **(a)** as well as proteins/transcripts related to beta-oxidation **(b)** and the glyoxylate cycle **(c)**. The horizontal line in the volcano plots indicates a p-value of 0.05; the horizontal and vertical lines in the ratio-*versus*-ratio plots indicate a $\log_2$fold-change of 0.

Pox1 produces hydrogen peroxide during β-oxidation, which is degraded by peroxisomal catalase (Cta1) [50]. In *pex3* cells, we found Cta1 to be upregulated at transcript and protein levels (**Figure 3b**). The peroxisomal Δ3-cis-Δ2-trans-enoyl-CoA isomerase Eci1 is required for the degradation of unsaturated fatty acids [51]. Previous work showed that Eci1 is co-imported with the $\Delta^{3,5}$-$\Delta^{2,4}$-dienoyl-CoA isomerase Dci1 [52], an enzyme involved in peroxisomal β-oxidation [53]. Since transcripts of its partner protein Dci1 (not identified on protein level) were not increased, Eci1 protein alone might not be stable and is therefore degraded in *pex3* cells (**Figure 3b**). In addition to the above mentioned β-oxidation enzymes, which all contain a PTS1, the essential PTS2 protein 3-ketoacyl-CoA thiolase (Pot1), which catalyzes the last step of each β-oxidation cycle, was upregulated to a similar extent at protein and transcript level (**Figure 3b**). Further upregulated peroxisomal enzymes were Lpx1 (a lipase) and Pcs60 (involved in oxalate degradation), but others (i.e. Bud16, Lys1, Str3) were unchanged (Figure S3). Interestingly, protein levels of the stress inducible peroxisomal enzymes Gpd1 (glycerol phosphate dehydrogenase) and Pnc1 (nicotinamidas) were not increased [54, 55], although both were transcriptionally downregulated (Figure S3).

To underscore our findings on the specific upregulation of β-oxidation enzymes, we also examined proteins of the glyoxylate cycle since it is another common and conserved function of yeast peroxisomes besides β-oxidation. Independent of their peroxisomal or cytosolic localization, transcripts and protein abundance of the known glyox-

ylate cycle enzymes were not affected by the deletion of *PEX3* (**Figure 3c**).

To conclude, in the absence of Pex3, central peroxisomal β-oxidation enzymes are upregulated at transcript and protein levels in acetate grown yeast cells. Exceptions are Eci1 and Pox1 exhibiting increased transcript but reduced protein levels in *pex3* cells, which most likely involves posttranslational mechanisms for their selective removal in peroxisome-depleted cells. The upregulation of β-oxidation enzymes might be linked to the increased abundance of the receptor proteins Pex5 and Pex7 and/or may be a direct cellular response to counteract the loss of functional peroxisomes.

The mitochondrial pyruvate carrier proteins Mpc1 and Mpc3 are so far unknown transporters of the peroxisomal membrane

Peroxisomal functions require the transport of ATP, nucleotides, and metabolites across the peroxisomal membrane. Thus, based on the metabolic pathways that occur in peroxisomes, numerous solute transporters are predicted to exist in the peroxisomal membrane, but only a few have been identified so far. We found that the peroxisomal adenine nucleotide transporter Ant1, which is involved in β-oxidation [56, 57] was markedly decreased at the protein but not transcript level in *pex3* cells (**Figure 4a**). Other known peroxisomal transporters involved in the import of activated long-chain fatty acids (Pxa1/2) and oligopeptides (Opt2) were only detected at the transcript level, without significant changes in *pex3* cells (**Figure 4a**; Table S1d).

Recent studies on *S. cerevisiae* peroxisomes [15] and mitochondria [58] showed that the proteomes of both organelles contain numerous multi-localized proteins. Thus, we hypothesized that solute transporters of other cellular compartments might partially localize to peroxisomes. The assumption that only a small fraction of these transporters reside in peroxisomal membranes would make it plausible that they have not been detected in peroxisomes so far. To further investigate this, we examined changes in protein and transcript levels of non-peroxisomal transporters in *pex3* cells (**Figure 4a**). Since known PMPs including Ant1 showed a significant decrease in protein but not transcript levels in *pex3* cells (**Figures 3a** and **4a**), we searched for proteins with similar behavior. This revealed two mitochondrial inner membrane carriers, Mtm1 and Mpc3. Mtm1 is a likely candidate for a peroxisomal transporter because it transports pyridoxal 5'-phosphate, which is produced by the putative pyridoxal kinase Bud16, an enzyme that localizes to the cytosol and peroxisomes [15]. Unfortunately, we could not detect Mtm1-GFP produced under the control of its endogenous promoter by FM.

We next tested the pyruvate carrier Mpc3 [59] (**Figure 4a**), one of three Mpc subunits (Mpc1-3) present in *S. cerevisiae*. Pyruvate is produced in yeast peroxisomes by the matrix enzyme Str3. Therefore, a pyruvate transporter is predicted to occur in the peroxisomal membrane. In respiring cells, Mpc3 forms a heterodimer with Mpc1 [60], whereas Mpc2 heterodimerizes with Mpc1 to form the fermentative mitochondrial pyruvate carrier (MPC) isoform [61, 62]. In our omics data, we quantified Mpc1, Mpc2, and Mpc3, with Mpc3 being significantly decreased in protein abundance (**Figure 4a**; Table S1d). Notably, Str3 levels were also reduced in *pex3* cells (Figure S3). Since Mpc1 is part of both MPC isoforms, a minor decrease in abundance due to the loss of peroxisomes might not be detectable in our experimental setting. To further test whether a portion of Mpc1 and Mpc3 localizes to peroxisomes in addition to their main localization in mitochondria, we performed FM analysis using proteins C-terminally tagged with GFP. As shown in **Figure 4b**, Mpc1 and Mpc3 predominantly localize to mitochondria, but a small fraction of these proteins is also present in small spots that harbor the peroxisomal marker protein Pex14. This is confirmed by the quantitative analysis of co-localization, which revealed a 60 % overlap of the Pex14-mCherry containing pixels with Mpc1-GFP and > 30 % for Mpc3 (**Figure 4c**).

Complementary to *S. cerevisiae*, *Hanensula polymorpha* is a methylotrophic yeast that is extensively used as a model organism in peroxisome research. *H. polymorpha* has two Mpc proteins, here called HpMpc1 (80.2 % similarity with ScMpc1) and HpMpc3 (73.4 % similarity to ScMpc3). To analyze whether the localization of a small portion of the Mpc proteins on peroxisomes also occurs in *H. polymorpha*, we checked the localization of the two *H. polymorpha* Mpc proteins. FM analysis showed that like in *S. cerevisiae*, both proteins have a mitochondrial and peroxisomal localization (**Figure 4d**). These results imply that the dual localization of Mpc proteins is conserved in different yeast species.

In contrast to Ant1, Mtm1 and Mpc3, we also detected transporters of increased protein abundance in *pex3* cells (**Figure 4a**). Tpo4 was one of the proteins with the highest change in abundance in *pex3* cells. Tpo1-4 are members of the major facilitator superfamily, localized in the vacuole and plasma membrane. We also detected Tpo1, 2 and 3, but only Tpo4 was significantly enhanced at the protein level. Tpo transporters are implicated in transport of various compounds, including drugs (Tpo1) [63, 64], polyamines (Tpo1-4) [65, 66], acetate (Tpo2 and Tpo3) [67] and medium chain fatty acids (Tpo1) [68]. Tpo1,2 and 3 have been extensively studied, however, Tpo4 is poorly characterized. FM analysis of a strain producing Tpo4-GFP revealed that the protein was predominantly present at the plasma membrane, but a portion of the protein localizes to the vacuole (**Figure 4e**). Tpo4-GFP did not co-localize with the peroxisomal marker protein Pex14. To investigate

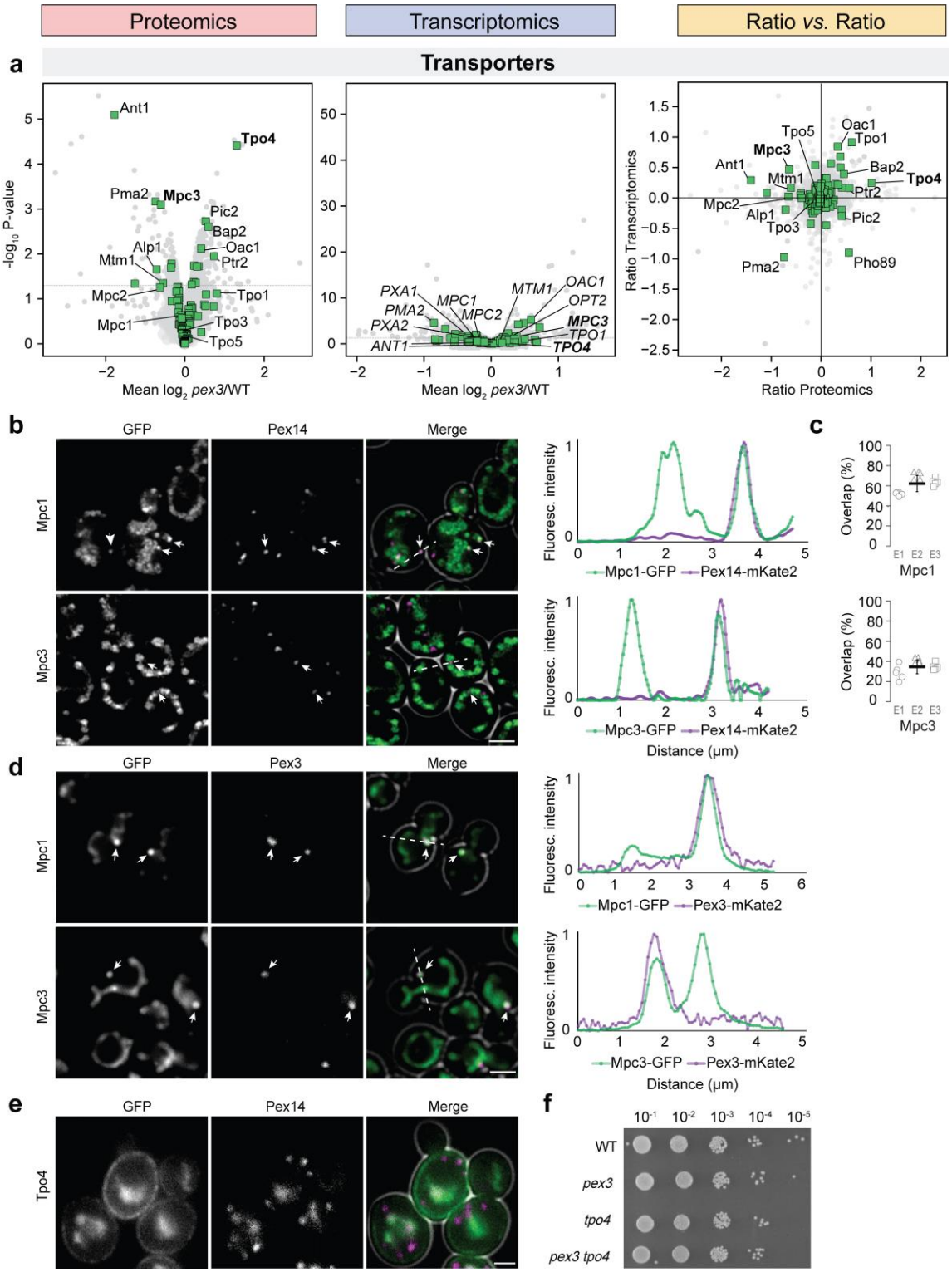

FIGURE 4 ● **Dual localization of Mpc proteins in yeast.** (a) Abundance of transporter proteins and transcripts in *pex3 versus* WT cells. The same plots as in Figure 3 highlighting transporters. (b) Airyscan fluorescence microscopy of acetate grown *S. cerevisiae* cells producing Mpc1-GFP or Mpc3-GFP under the control of their endogenous promoters. Pex14-mCherry was used as a peroxisome marker. The cell contour is shown in white. Scale bar: 2.5 µm. Graphs show normalized fluorescence intensity along the lines indicated in the merged images. (c) Quantitative co-localization analysis of Pex14-mCherry and Mcp1 or Mpc3 with Manders' Overlap Coefficient. Each data point represents one image with approximately 50 cells of three independent experiments (E1, E2, E3). The line represents the average, error bars represent the standard deviation (SD). (d) FM analysis of glucose grown *H. polymorpha* cells producing Mpc1-GFP and Mpc3-GFP under the control of the *ADH1* promoter. Pex3-mKate2 was used as a peroxisome marker. The cell contour is shown in white. Scale bar: 2.5 µm. Graphs show normalized fluorescence intensity along the lines indicated in the merged images. (d) FM analysis of acetate grown *S. cerevisiae* cells producing Tpo4-GFP under the control of its endogenous promoter. Pex14-mCherry was used as a peroxisome marker. The cell contour is shown in white. Scale bar: 1.5 µm. (d) Growth analysis of WT and the indicated (double) deletion strains. Spot assays were performed using a mineral medium containing 0.5% acetate. Cultures were serially diluted (from 10^{-1} to 10^{-5}) and spotted on agar plates. A representative spot assay of 2 independent experiments is shown.

the correlation between Tpo4 and peroxisomes, we analyzed growth on acetate using a spot assay. As shown in **Figure 4f**, the *tpo4* single and *tpo4 pex3* double deletion strains showed similar growth. This indicates that enhanced Tpo4 levels are not crucial for the growth of *pex3* cells on acetate.

In sum, we investigated transporters with significant changes at the protein level. While for Tpo4 we did not find any direct correlation with peroxisomes, our investigation of the pyruvate carriers Mpc1 and Mpc3 revealed that a portion of these proteins is detectable at some of the peroxisomes.

Functional classification of regulated non-peroxisomal transcripts and proteins in *pex3* cells

Our omics analysis of *pex3* cells revealed that peroxisomal membrane-localized peroxins (except for Pex22 and Pex8) were decreased in abundance. Previous work showed that Pex11 is detectable on mitochondria in yeast *pex3* and/or *pex19* cells [27, 69]. Thus, in the absence of peroxisomes, PMPs are degraded or localize to another subcellular niche. In yeast, all peroxisomal proteins are synthesized in their mature form and folded in the cytosol prior to import. However, the upregulation of abundant peroxisomal β-oxidation enzymes might challenge cellular proteostasis and the loss of peroxisomal functions might elicit metabolic changes. To obtain information about the existence of such cellular responses, we next investigated non-peroxisomal transcripts and proteins in *pex3* cells.

Pex3 deficiency results in altered levels of various factors of non-peroxisomal metabolic pathways. We assessed changes in the levels of non-peroxisomal transcripts and proteins in *pex3* cells (**Figure 5**). We reanalyzed the LoQAtE database [70] for information about the subcellular localization of all 54 non-peroxisomal proteins with altered protein or transcript abundance in *pex3* cells. Manual inspection of the images in the database revealed that 14 of these (marked in Table S1c) show a "punctate" distribution (which could suggest a peroxisomal localization) or "punctate" in addition to another localization such as mitochondria, ER, or nucleus. This could indicate that non-peroxisomal proteins affected in *pex3* cells may be localized to multiple cellular niches with a partial localization in peroxisomes, which may vary depending on the metabolic condition of the cells. However, so far, none of the 14 proteins with punctate distribution has been associated with peroxisomes or peroxisomal functions.

Many of the regulated non-peroxisomal transcripts that encode proteins whose levels were unchanged are uncharacterized ones (Table S1d), and that is why we do not discuss them further. Among the characterized regulated transcripts, we found a strong transcriptional upregulation of *EEB1*, which is involved in the biosynthesis of medium-chain fatty acid ethyl ester under fermentative growth [71], and two helicases (YBL113C, YBL111C), but none of their translation products was identified in our proteomics analysis (**Figure 5a**; Table S1d). Upregulated transcripts that displayed a slight increase at the protein level include the cytosolic proteins inositol-3-phosphate synthase (Ino1) and Leu1, which is essential for leucine biosynthesis, as well as the branched-chain amino acid aminotransferase Bat1, and the oxaloacetate carrier Oac1 (**Figure 5a**).

Among the downregulated transcripts that were also reduced at protein level were the plasma membrane H^+-ATPase Pma2, an aldehyde reductase (Ykl107w), glyceraldehyde-3-phosphate dehydrogenases (Tdh1; Tdh2, 1.3-fold up), a spore wall maturation associated protein (Sps100), the general stress responsive factor Gre1, as well as the pentose phosphate pathway enzymes 6-phosphogluconate dehydrogenase (Gnd2) and transketolase (Tkl2). Furthermore, transcripts of the plasma membrane protein Ynl194c and its paralog Fmp45, which both are involved in sphingolipid metabolism [72], were considerably downregulated (**Figure 5a**).

We next examined regulated non-peroxisomal proteins, which were in many cases not affected at transcript level in *pex3* cells (**Figure 5b**). Interestingly, this included a few proteins related to nitrogen metabolism (Uga3, Gzf3, Dur12). Both Uga3 and Gzf3 are enhanced at the protein level. Uga3 and Gzf3 are transcription factors involved in the regulation of genes involved in the uptake and utilization of non-preferred nitrogen sources [73]. One of the Gzf3 regulated genes is urea amidolyase Dur12 (alias Dur1,2) [74-76], which had a lower abundance in the *pex3* cells. Since ammonium is the nitrogen source in the medium used, it is not directly conceivable why proteins involved in the utilization of alternative nitrogen sources were changed.

Loss of Pex3 leads to increased levels of specific chaperones ensuring protein folding. Among the proteins of decreased abundance were Ubx5, Snf6, and Hsp26. Ubx5 is an adapter of the AAA ATPase Cdc48/p97 [77] and involved in the degradation of proteins by the proteasome [78-80]. The downregulation of the nuclear protein Snf6, which is involved in transcriptional activation [81, 82], generally fits the observation that *pex3* cells do not show widespread changes in their transcriptional program. The small heat shock protein Hsp26 is involved in the reactivation of misfolded, aggregated proteins by Hsp104 [83]. Like the stress factor Gre1, Hsp26 was transcriptionally downregulated (**Figure 5b**). Furthermore, *PEX3* deletion resulted in decreased transcripts but unaltered protein levels of the disaggregase Hsp104 and the sequestrase Hsp42 (Table S1d), which both fulfill vital roles in maintaining proteostasis in *S. cerevisiae* [84-86]. However, we found an increase in the abundance of Hsp12 and Hsp31 (1.4-fold up) (**Figure 5b**). Hsp12 is involved in plasma membrane organization during stress

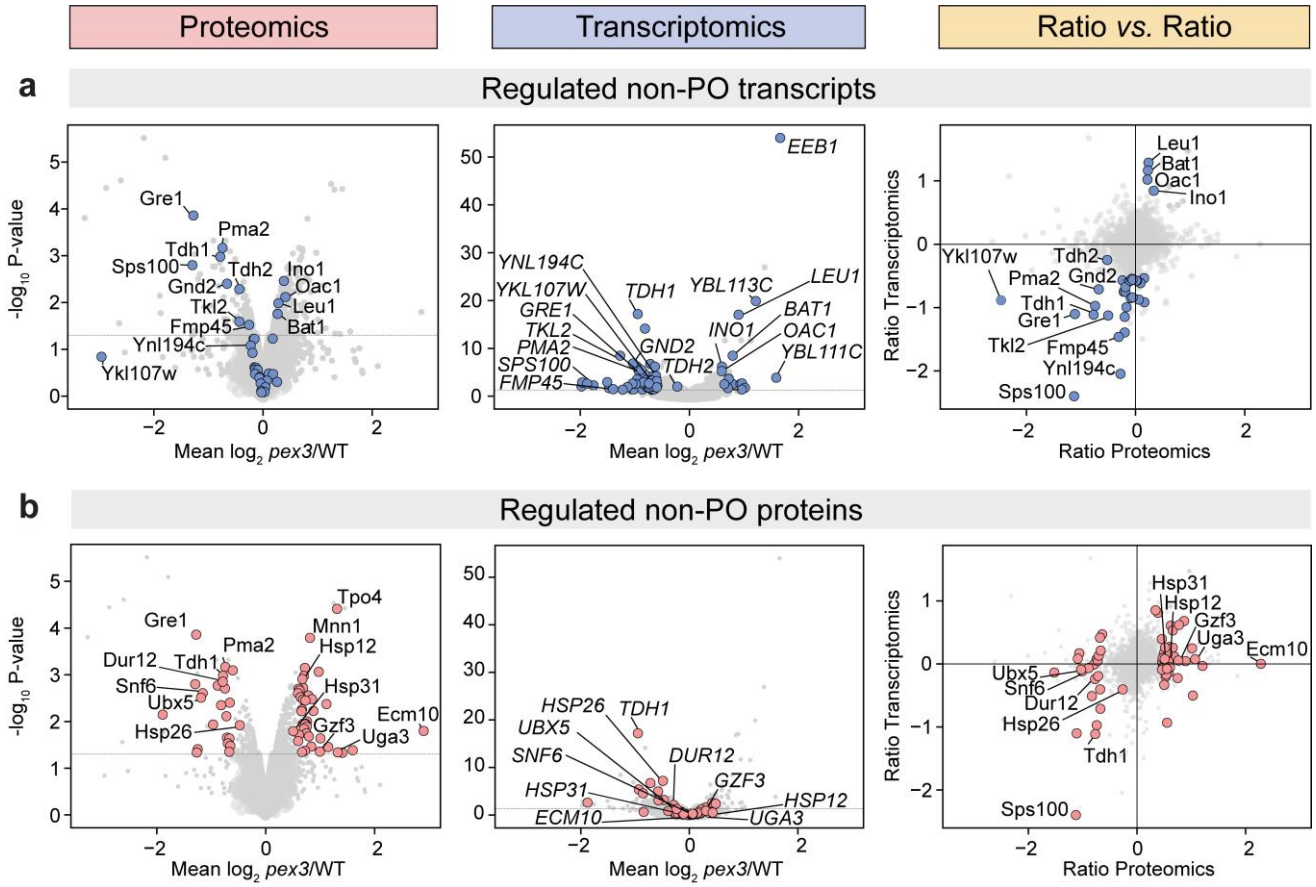

FIGURE 5 ● **Effect of *PEX3* deletion on transcripts and proteins not previously linked to peroxisomal processes.** Same plots as in Figure 3. Highlighted are (a) regulated transcripts unrelated to peroxisomal (PO) processes and the corresponding proteins and (b), *vice versa*, regulated non-peroxisomal proteins and the corresponding transcripts. Transcripts/proteins with a minimum fold-change of ± 1.5 and a p-value of < 0.05 (n=3) are highlighted in blue/red, as well as the TDH2 transcript.

[87, 88], whereas Hsp31 protects cells from protein misfolding stress at an early state to prevent protein aggregation [89]. Thus, our data indicate that early protective responses to mitigate protein misfolding are active and likely enable cells to maintain proteostasis in the absence of peroxisomes.

Most interestingly, we observed the highest increase in abundance for the mitochondrial matrix protein Ecm10 in *pex3* cells, whereas transcripts remained unchanged (**Figure 5b**). Ecm10 is a member of the mitochondrial Hsp70 protein family. Further family members are Ssc1 and Ssq1 (reviewed in [90]). Ssc1 is involved in the import and folding of mitochondrial precursor proteins and Ssq1 in iron-sulfur protein biogenesis, but neither of them was regulated in *pex3* cells. Other mitochondrial chaperones (e.g. Hsp60, Hsp78, Hsp10) were also not changed in abundance (Table S1d). Notably, Ecm10 is a paralog of Ssc1, and supposedly also involved in the import and folding of newly synthesized precursor proteins in the mitochondrial matrix [91]. Based on this unexpected specific mitochondrial response manifested by highly increased Ecm10 levels, we examined in more detail changes in the abundance of mitochondrial proteins in *pex3* cells which lack peroxisomes.

Proteins with a central role in mitochondrial respiration and import are increased in *pex3* cells. Mitochondria fulfill central metabolic functions highlighted by the production of ATP by oxidative phosphorylation [58, 92]. In *pex3* cells, most mitochondrial transcripts were unaltered in abundance, except for the downregulated transcripts of the Sdh3 and Sdh4 homologs Shh3 and Shh4 or upregulated transcripts of the oxaloacetate carrier protein Oac1 and mitochondrial aldehyde dehydrogenase Ald5, which plays a role in the biogenesis of the electron transport chain and synthesis of acetate [93, 94] (Figure S4a). On the proteome level, we found an increase in the abundance of numerous proteins that are associated with central mitochondrial protein machineries in *pex3* cells. We found a higher abundance of proteins with a role in the assembly and function of mitochondrial respiratory chain complexes (**Figure 6**). These included (i) different subunits (Atp18, Atp15, Atp14) of the mitochondrial F1F0 ATP synthase, (ii) the twin ATPase regulators Inh1 and Stf1 that inhibit uncoupled ATP hydrolysis [95], (iii) assembly factors (Cox19,

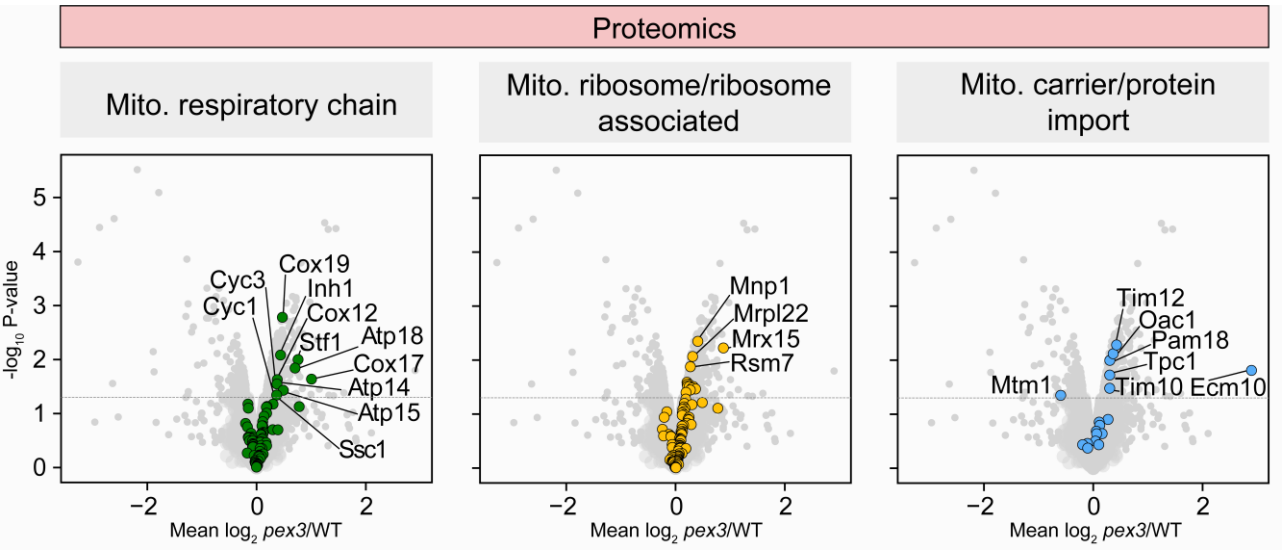

FIGURE 6 ● **Changes in the abundance of mitochondrial proteins in *pex3* cells.** The same volcano plots as in Figure 2b highlighting components of the mitochondrial (mito.) respiratory chain (left), mitochondrial ribosomal and ribosome-associated components (middle), and proteins associated with the mitochondrial carrier import pathway or involved in the mitochondrial presequence import pathway (right).

Cox17, Cox12) of mitochondrial cytochrome c oxidase [96-99], and (iv) cytochrome c isoform 1 (Cyc1) and cytochrome c heme lyase Cyc3, which attaches heme to apo-Cyc1 [100].

The mitochondrial respiratory chain is of dual-genetic origin and therefore its assembly requires the insertion of nucleus- and mitochondria-encoded subunits into the inner mitochondrial membrane (IMM). Interestingly, *pex3* cells exhibited higher levels of Dpi29 [58], alias Mrx15 (**Figure 6**). It is a receptor of mitochondrial ribosomes required for the efficient co-translational insertion of mitochondria-encoded membrane proteins into the IMM [101]. Moreover, proteins of mitochondrial ribosomes were generally shifted towards higher abundance in *pex3* cells, which was most pronounced for Mnp1, Mrpl22 or Rsm7 (**Figure 6**). In addition to mitochondria-encoded proteins, also nucleus-encoded hydrophobic metabolite carriers need specific guidance for their delivery to the carrier translocase TIM22 in the IMM [92]. In *pex3* cells, the abundance of the mitochondrial carrier proteins Oac1 and Tpc1 was increased, along with higher levels of Tim10 and Tim12, which deliver, together with Tim9, carrier proteins to the carrier translocase TIM22 in the IMM (**Figure 6**). Levels of the J-protein cochaperone Pam18 were also increased, which is an essential subunit of the presequence-associated motor of the translocase of the inner mitochondrial membrane (TIM23) [92]. Specifically, Pam18 facilitates the import of mitochondrial presequence proteins into the mitochondrial matrix by stimulating the ATPase activity of the Hsp70 family ATPase Ssc1 [102]. Notably, levels of Ecm10, but not Ssc1, were highly increased, which points to a role of Ecm10 in mitochondrial protein import under peroxisome-deficient conditions.

Moreover, the abundance of the integral ER membrane protein Ylr050C, alias Ema19, and the intramembrane aspartyl protease of the perinuclear ER membrane (Ypf1) were also increased in cells lacking Pex3 (Figure S4b). Ema19 is involved in the ER surface retrieval pathway (ERSURF) to effectively target membrane proteins to the mitochondrial surface for import [103] and has been identified as a quality control factor for newly synthesized but unstable mitochondrial precursor proteins [104]. Ypf1 is a protease that is involved in a branch of the endoplasmic reticulum unfolded protein response (ERAD) [105].

To conclude, our omics data show that the absence of Pex3 in acetate grown yeast cells does not elicit major changes in the transcriptional program and changes in protein levels are therefore mainly governed by posttranscriptional mechanisms. Our proteomics data further indicate that the absence of peroxisomes in *pex3* cells leads to changes in the abundance of specific factors that play important roles in mitochondrial respiration, protein import and the folding of mitochondrial precursors in the mitochondrial matrix.

DISCUSSION

Here, we report a comprehensive whole cell transcriptome and proteome study to uncover the effects of the absence of peroxisomes in yeast cells by comparing WT and peroxisome-deficient *pex3* cells. We show that the absence of peroxisomes elicits specific cellular responses (for an overview see **Figure 7**). Key observations include (1) upregulation of almost all peroxisomal β-oxidation enzymes at both transcript and protein level, (2) unchanged expression of *PEX* genes at the transcript level but reduced levels of all peroxins except for Pex5 and Pex7, which

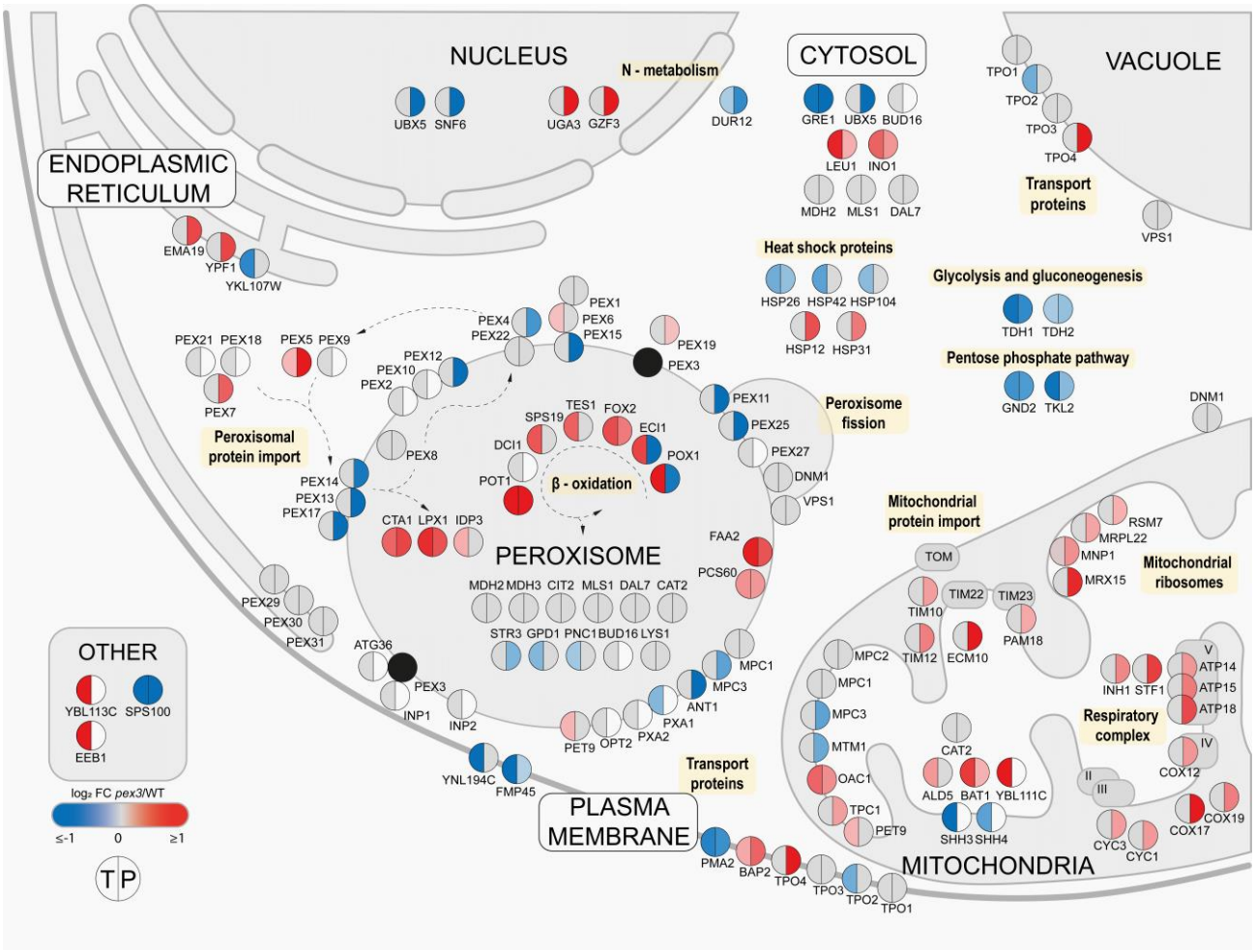

FIGURE 7 ● Overview of changes in the transcriptome and proteome of *pex3* versus WT cells. Shown are transcripts/proteins discussed in the results section and their subcellular localization (based on literature, the *Saccharomyces* Genome Database and/or UniProt). Circles represent the transcripts (T, left) and proteins (P, right). Transcripts/proteins that fulfill the p-value threshold of < 0.05 are colored. Unchanged and undetected transcripts/proteins are depicted in gray and white, respectively. Category "other" includes candidates with unknown localization.

were considerably increased in abundance, (3) downregulation of several genes encoding proteins involved in various non-peroxisome-related cellular processes [e.g. pentose phosphate pathway (PPP), plasma membrane transporters] in *pex3* cells, and (4) higher levels of specific mitochondrial proteins without change in transcript levels (Figure 7).

Growth of *pex3* cells on acetate and glyoxylate cycle enzymes

We used yeast *pex3* cells, which lack peroxisomes, as a model system. Peroxisome-deficient yeast mutants are viable [106], while the complete absence of any other cell organelle is lethal in yeast. This unique feature was the basis of our study. To detect changes that were exclusively caused by the absence of peroxisomes, it was imperative to use conditions that do not affect cell growth or repress genes encoding proteins involved in peroxisome biology. We showed that growth on acetate fulfils these criteria. In addition, under these conditions, peroxisomes harbor enzymes of the glyoxylate cycle [28], which are essential for the growth on acetate [31, 107]. Our data revealed that glyoxylate cycle enzymes were unchanged at transcript and protein level in *pex3* cells. Apparently, these cytosolically mislocalized enzymes are sufficiently active to allow *S. cerevisiae* yeast cells to grow on acetate. This is in line with the early observation that *S. cerevisiae pex* mutants can grow on non-fermentable carbon sources such as acetate and are only defective in the utilization of oleic acid [106].

Changes in the transcriptome of *pex3* cells and potential links to ERAD

Despite the absence of peroxisomes, the transcriptome of *pex3* cells hardly changed overall. Only 102 out of 5,460 detected transcripts were altered more than ±1.5-fold (p-value < 0.05), which is less than 2%. Also, only 17 out of the 123 transcripts encoding peroxisomal proteins signifi-

cantly changed (p-value of < 0.05), with 9 showing a fold-change of > ±1.5. Similar observations were made in transcriptomic studies using other *S. cerevisiae pex* mutants (*pex12*; microarray analysis [108] or *pex19*; RNAseq [2]). Notably, for *S. cerevisiae pex12* cells a more than 1.5-fold upregulation of seven genes involved in lysine biosynthesis was reported. We did not observe changes in any of these transcripts in *S. cerevisiae pex3* cells. Most likely, this is due to differences in growth conditions (glucose instead of acetate, i.e. fermentative versus non-fermentative conditions) or the method used (RNA-seq versus microarrays). Nuebel and colleagues observed that three zinc-response genes (*ADH4*, *ZAP1*, *ZRT1*) were downregulated in *S. cerevisiae pex19* cells. The transcripts of none of these genes were significantly changed in our study using acetate grown *pex3* cells. In *pex19* cells, *ULI1* transcripts were reduced as well [69]. Uli1 is a protein of unknown function that is induced by the ERAD pathway [109-111]. In *pex3* cells, we found higher levels of the protease Ypf1, which is involved in the selective degradation of functional proteins as part of a distinct branch of ERAD and was shown to regulate the levels of nutrient transporters during starvation [105]. Thus, it might be involved in regulating protein levels in yeast cells lacking Pex3. Another ERAD related protein that was altered in our study is Ubx5, an adaptor of the Cdc48 machine in ERAD [77]. In the study of *pex19* cells by Nuebel and colleagues [69], the growth conditions were quite different from what we used (i.e. growth on a mixture of ethanol and glycerol and harvesting of cells from the stationary growth phase), which may explain the differences in observations.

Changes in the proteome of *pex3* cells and identification of Mpc1/Mpc3 as dual-localized transporters

Like for transcripts, also a rather small fraction of the entire proteome was changed in *pex3* cells. Out of the 92 detected peroxisomal proteins, 17/11 were reduced/increased in abundance (p-value < 0.05). Strikingly, almost all known PMPs, which include peroxins and the peroxisomal transporter Ant1, had a reduced abundance in *pex3* cells. This is in agreement with earlier studies, which revealed that newly synthesized PMPs were rapidly degraded in *S. cerevisiae pex3* cells [24]. The instability is most likely due to the fact that PMP sorting is abolished. Like for PMPs, the mitochondrial pyruvate carrier Mpc3 was also significantly reduced in abundance in *pex3* cells (fold-change 0.66), which might indicate a dual localization on peroxisomes and mitochondria. This option was also inspired by recent reports on the dual localization of two other mitochondrial inner membrane carriers on peroxisomes and mitochondria *S. cerevisiae* Pet9, alias Aac2 [112] and *H. polymorpha* Mir1 [113]. Moreover, although a peroxisomal pyruvate transporter was predicted to exist, due to the presence of the pyruvate producing enzyme Str3 in the matrix, it was never identified. Indeed, we established the dual localization of the heterodimeric Mpc1/Mpc3 pyruvate carrier to peroxisomes and mitochondria. This suggests that multiple mitochondrial carriers may be dually localized. Only a small fraction of Mpc1/Mpc3 was observed at a subset of the peroxisomes, which likely explains why the peroxisomal localization was missed in other studies, like high throughput FM [15] or organelle proteomics [16]. The presence of peroxisomal proteins in subdomains or on a subset of the peroxisomal population has also been reported before for other proteins [15, 114].

Upregulation of β-oxidation enzymes and links to cellular responses

In *S. cerevisiae*, expression of β-oxidation enzymes and Cta1 are known to be induced under peroxisome proliferation conditions. This effect is most pronounced for PTS1 and PTS2 enzymes whose expression is strongly inducible when peroxisome functions are needed [115]. In acetate grown yeast cells, genes encoding β-oxidation enzymes are derepressed [32]. Notably, all 9 peroxisomal transcripts that were considerably enhanced in *pex3* cells encode peroxisomal β-oxidation enzymes and most of them were also increased at the protein level (**Figure 7**). In *pex3* cells, the β-oxidation pathway is most likely much less active due to the cytosolic mislocalization of the enzymes together with the lower abundance of Eci1 and Pox1, which produce the first product of the β-oxidation pathway [51, 116]. This will reduce the flux through the entire cascade of β-oxidation reactions. As a result of the reduction in β-oxidation, the levels of free fatty acids may increase, leading to further induction of the expression of the genes encoding β-oxidation enzymes. The upregulation of β-oxidation enzymes might also be linked to the increased abundance of the receptor proteins Pex5 and Pex7 and/or may be a direct cellular response to counteract the loss of peroxisomes. In contrast, the considerably reduced Pox1 protein levels in *pex3* cells may explain why transcripts/proteins of the cellular oxidative stress response were unchanged. The reduced levels of Pox1 may be related to regulation by Arf1, which specifically controls its protein but not transcript levels [22]. Possibly, Eci1 protein levels are controlled by the same mechanism. Our data further show that high levels of mislocalized β-oxidation enzymes is accompanied by enhanced levels of Hsp12 and Hsp31, which both play a role in early responses to prevent protein misfolding. Based on these findings, we hypothesize that such upregulated β-oxidation enzymes are stabilized in their folded state by chaperones (e.g. Hsp31) in the cytosol and may therefore prevent the formation of aggregates in *pex3* cells. This might also explain why levels of the molecular chaperone Hsp26, the disaggregase Hsp104, and the sequestrase

Hsp42 were transcriptionally reduced in *pex3* cells. However, this transcriptional decrease was not reflected in Hsp104 and Hsp42 protein levels, which remain unaltered in pex3 cells. The latter finding may indicate their stabilization at a posttranslational level in these mutant cells. Nevertheless, further work is needed to better understand the different effects that mislocalized peroxisomal proteins have on the cellular proteostasis system.

Alterations of non-peroxisomal proteins and transcripts in *pex3* cells and links to different metabolic pathways

The absence of peroxisomes in *pex3* cells not only resulted in changes in peroxisome related transcripts or proteins. Interestingly, levels of several mitochondrial proteins were enhanced (**Figure 7**). These included proteins involved in mitochondrial respiration, protein import and protein refolding in the matrix. This may shed new light on the functional interactions between both cell organelles and may indicate that specific processes for safeguarding the fitness of mitochondria are induced in *pex3* cells. Moreover, it may give new hints to better understand the molecular mechanisms behind mitochondrial changes in peroxisome deficient human cells [69, 117, 118].

Another example of a non-peroxisomal protein with an increased abundance in *pex3* cells is Tpo4 (a transporter of the major facilitator superfamily), but further analysis is needed to reveal why this PM/vacuole transporter is enhanced in the absence of Pex3. Also, genes that were strongly enhanced are very attractive for further analysis. The transcript with the highest increase in *pex3* cells is EEB1. This gene encodes acyl-coenzymeA:ethanol O-acyltransferase, which is implicated in lipid metabolism and detoxification [71].

Our study further revealed that a large variety of poorly characterized proteins were reduced both at the transcript and protein level (e.g. Gre1, Sps100, Ykl107w). In addition, transcripts/proteins related to glucose metabolism, e.g. Tdh1 and Tdh2 (glyceraldehyde-3-phosphate dehydrogenases), Gnd2 6-phosphogluconate dehydrogenase) and Tkl2 (transketolase) were downregulated as well as Pma2 (a plasma membrane ATPase). Notably, Gnd2 is a dually localized enzyme in the cytosol and peroxisomes in rat liver [119]. Furthermore, the role of Ykl107w, a member of the classical short-chain dehydrogenase/reductase family, in peroxisomal β-oxidation is conceivable. Thus, both enzymes are promising candidates for studying their potential function in peroxisome biology.

A few changes were also observed in proteins involved in the metabolism of non-preferred nitrogen sources. This includes enhanced protein levels of two transcription factors (Uga3 and Gzf3) that regulate genes involved in the uptake of these nitrogen sources. The amidolyase Dur12 is also regulated by Gzf3, however, the abundance of this protein was reduced in *pex3* cells. These data imply that in the absence of peroxisomes nitrogen metabolism has changed. This is intriguing because so far enzymes involved in nitrogen metabolism have not been reported to exist in *S. cerevisiae* peroxisomes. This is different to other yeast species, which contain several peroxisomal enzymes involved in the oxidation of organic nitrogen sources (e.g. amine oxidase, D-amino acid oxidase and urate oxidase in *H. polymorpha* [120]). Moreover, such enzymes also occur in peroxisomes of higher eukaryotes including plants [121] and mammals [122].

Concluding remarks

We here show that the comparison of the whole cell proteome and transcriptome of a yeast *pex* mutant is a powerful approach to identifying novel processes and pathways influenced by peroxisomes. It would be interesting to also study other *pex* mutants that are not defective in PMP sorting, but in other processes. Attractive candidates include a *pex5 pex7* double mutant, which is selectively blocked in matrix protein import, or mutants that show defects in other aspects of peroxisome biology such as peroxisome fission (Pex11), peroxisome-ER contact site formation (Pex30), peroxisome inheritance (Inp1) or pexophagy (Atg36). Another option is to compare different pex mutants. Comparison of *pex3* and *pex19* cells may uncover new Pex3 or Pex19 functions. We already know that Pex3 is a multitasking protein that is also important for pexophagy by recruiting Atg36 and for peroxisome inheritance by recruiting Inp1 [123, 39]. In mammals, Pex19 is implicated in alternative functions unrelated to peroxisomes [124-126]. A comparison of *pex3* and *pex19* cells may therefore give novel hints to additional functions of these important peroxins in yeast.

Summarizing, we here show the power of the comparison of the whole cell proteome and transcriptome of a WT and peroxisome-deficient yeast mutant. The data obtained resulted in the identification of Mpc1/Mpc3 as another example of a dually localized mitochondrial carrier protein. Moreover, we uncovered many proteins/transcripts and cellular processes that have so far not been connected with peroxisome biology.

MATERIAL AND METHODS

Strains and growth conditions

The yeast strains used in this study are listed in Table S3. Yeast cells were grown in batch cultures on a mineral medium (MM) [127] supplemented with 0.5% glucose or 0.5% acetate. When required, amino acids were added to the media at the following concentrations: 20 mg/L histidine, 30 mg/L leucine, 20 mg/L methionine, and 30 mg/L uracil. *S. cerevisiae* was grown at 30°C, *H. polymorpha* at 37°C.

For the selection of transformants, plates were prepared with 2% agar in YPD (1% yeast extract, 1% peptone, and 1% glucose) supplemented with 100 μg/mL zeocin

(Invitrogen), 300 μg/mL hygromycin B (Invitrogen) or 100 μg/mL nourseothricin (Werner Bioagents).

S. cerevisiae cells were grown overnight in MM containing glucose, shifted to MM containing glucose, and shifted two times to MM containing acetate. For the analysis of (i) growth on acetate, the optical density of the cultures was measured at OD_{660} every 4 h with starting OD_{660} =0.1, (ii) acetate consumption, media was harvested at time points 0 h, 8 h, 12 h and 21 h, corresponding to OD_{660} of approximately 0.1, 0.5, 1.0 and 2.3 respectively; (iii) whole cell proteome and transcriptome, cells were harvested when cultures reached an OD_{660} of 0.5. For FM analysis *S. cerevisiae* cells were grown overnight in MM containing glucose, shifted to MM containing acetate twice, and imaged when reaching OD_{660} = 0.8-1.0. For spot assay, *S. cerevisiae* cells were grown overnight in MM containing glucose and shifted to MM containing acetate twice. When cells reached the OD_{660} = 1, serial dilutions were made (10-1, 10-2, 10-3, 10-4, 10-5) and spotted on mineral medium plates containing acetate (0.5%). Plates were incubated at 30°C. Spot assays to test growth on oleate-containing agar plates were performed as described previously [19]. Cells were plated on appropriate selection medium.

H. polymorpha cells were grown overnight in MM containing glucose, shifted to MM containing glucose twice, and imaged when reaching OD_{660} = 0.8-1.0.

Measurement of acetic acid concentrations

Acetic acid was analyzed by HPLC equipped with a refractive index detector (Shimadzu, Kyoto, Japan) using an Aminex HPX-87H column (Bio-Rad) at a temperature of 65°C using a mobile phase of 0.005 N H2SO4 and a flow rate of 0.55 mL/min.

Construction of *S. cerevisiae* strains

S. cerevisiae strains retrieved from different yeast libraries (Euroscarf) [107. 128-130] were confirmed with PCR. To construct strains producing Pex14-mCherry, a PCR fragment encoding Pex14-mCherry was obtained using primers TER214 and TER215. Upon transformation, correct integration was confirmed by colony PCR using TER216 and R-mCherry-CP.

To obtain *S. cerevisiae pex3* strains containing P_{NOP1} sfGFP-Mdh3, P_{NOP1} sfGFP-Cat2 and P_{NOP1} sfGFP-Cit2, a deletion cassette was amplified with primers F-Pex3-del and R-Pex3-del using pUG6 as a template and introduced in the corresponding WT strains. Replacement of the genomic gene in the *S. cerevisiae* strains by the deletion cassette was confirmed by colony PCR, using primers F-Pex3pr-del-CP, R-KanMX-CP and R-Pex3-del-CP.

To obtain the *TPO4* deletion strains, a deletion cassette was amplified with primers F-Tpo4-del and R-Tpo4-del using pHIPH4 as a template. Replacement of the genomic *TPO4* gene in the *S. cerevisiae* strains with deletion cassette was confirmed with the colony PCR, using primers F-Tpo4-del-CP and R-Tpo4-del-CP, and Southern blotting.

Plasmid pHIPZ Tpo4 3xHA was obtained from GenScript, and constructed as follows: C- terminal fragment Tpo4 with 3xHA tag was synthesized and inserted into the pHIPZ mGFP-fusinator between *Hind*III and *Sph*I restriction sites. *Sfu*I restriction site was introduced to the fragment Tpo4 3xHA with silent mutation 1893C>G. *Sfu*I linearized pHIPZ Tpo4 3xHA was integrated into the *TPO4* gene of *S. cerevisiae* WT and *pex3* deletion strain. Gene integration was confirmed with colony PCR using primers F_Tpo4 3xHA and pHIPZ-pHIPZ5 rew seq.

The PCR-based cloning approach and transformation of *S. cerevisiae* strains using the lithium acetate method were performed as previously described [131].

Construction of *H. polymorpha* strains

To find homologs of Sc Mpc1 and Mpc3, we performed the blastp (NCBI) using all non-redundant protein sequence (nr) database in *H. polymorpha* (taxid:870730) and blastN, standard database in Ogataea (taxid:461281) (date used 6.3.2023). Two genes/proteins with the accession KAG7879638 and XP_013933851 were found, called here HpMpc1 and HpMpc3.

Plasmid pHIPZ18 Mpc1-meGFP was obtained as follows: PCR was performed on *H. polymorpha* WT genomic DNA using primers MPC1-C-fw and MPC1-C-rev. The PCR product was digested with *Hind*III and *Bam*HI, and inserted between the *Hind*III and *Bgl*II sites of the pHIPZ18 Inp1-meGFP. *Eco*RI linearized pHIPZ18 Mpc1-meGFP was integrated into the *ADH1* promoter of *H. polymorpha* yku80 producing Pex3 mKate2, resulting in strain Hp P_{PEX3} Pex3-mKate2::P_{ADH1} Mpc1-meGFP. Gene integration was confirmed with colony PCR using primers cPCR MPC1-Cfw and mGFP rev check.

Plasmid pHIPZ18 Mpc3-meGFP was obtained as follows: PCR was performed on *H. polymorpha* WT genomic DNA using primers MPC3-C-fw and MPC3-C-rev. The PCR product was digested with *Hind*III and *Bgl*II, and inserted between the *Hind*III and *Bgl*II sites of the pHIPZ18 Inp1-meGFP. *Eco*RI linearized pHIPZ18 Mpc3-meGFP was integrated into the *ADH1* promoter of *H. polymorpha* yku80 producing Pex3 mKate2, resulting in a strain Hp P_{PEX3} Pex3-mKate2::P_{ADH1} Mpc3-meGFP. Gene integration was confirmed with colony PCR using primers cPCR MPC3-Cfw and mGFP rev check.

Transformations and site-specific integrations were performed as described previously [132].

Cell lysis for proteomics analysis and proteolytic digestion

Cells were harvested by flash cooling the culture flasks on wet ice for 5 min followed by centrifugation for 7 min at 6000 g and 4°C. After harvesting, *S. cerevisiae* cells were washed once with deionized H2O, resuspended in 500 µL of urea buffer (8 M urea, 75 mM NaCl, 50 mM Tris-HCl, pH 8.0), and lysed by bead beating using a Minilys homogenizer (three cycles of 2 min at 4,000 rpm with 2 min cooling on ice between the cycles). For removal of cell debris, lysates were centrifuged for 5 min at 15,000 g and 4°C. Supernatants were collected and protein concentrations were determined using the bicinchoninic acid assay [133].

500 µg of protein per sample were treated with tris (2-carboxyethyl)phosphine (5 mM final concentration; 30 min at 37°C) to reduce cysteine residues followed by alkylation of free thiol groups using iodoacetamide (50 mM; 30 min at room temperature in the dark). Proteins were subsequently digested in solution using LysC and trypsin as previously described [134]. Peptides were desalted using solid-phase extraction microspin disk cartridges (Affinisep, Le Houlme, France) that had been conditioned with methanol followed by 80% (v/v) acetonitrile (ACN)/0.5% (v/v) acetic acid and 0.5% (v/v) acetic acid. Peptides were loaded onto the cartridges, washed twice with 0.5% (v/v) acetic acid and eluted using 80% (v/v) ACN/0.5% (v/v) acetic acid. Solvents were evaporated and dried peptides were stored at -20°C until further use.

Peptide stable isotope dimethyl labeling

Peptides (300 µg per sample) derived from WT and *pex3* cells were differentially labeled with 'light' formaldehyde (CH_2O) and sodium cyanoborohydride ($NaBH_3CN$) or the corresponding deuterated 'heavy' reagents (CD_2O and $NaBD_3CN$) as described before [43, 135]. Experiments were performed in three independent biological replicates. In replicate 1, peptides of WT and *pex3* cells were labeled 'light' and 'heavy', respectively. In replicates 2 and 3, the labeling was reversed to account for potential labeling bias. The labeling efficiency, assessed by LC-MS analysis, was > 97%. Equal amounts of differentially dimethyl-labeled peptides of WT and *pex3* cells (100 µg each) were mixed and dried in vacuo.

High pH reversed-phase fractionation

To achieve high proteome coverage, peptide mixtures were fractionated using high pH reversed-phase liquid chromatography (LC) [136] as described before [137]. In brief, dried peptides were reconstituted in 100 µL of 99% solvent A (10 mM ammonium hydroxide, pH 10) and 1% solvent B (10 mM ammonium hydroxide in 90% ACN, pH 10), insoluble material was removed by centrifugation (12,000 x g, 5 min, room temperature), supernatants were filtered through a 0.2 mm PTFE membrane syringe filter (Phenomenex, Torrence, USA), and peptide mixtures were separated on an NX 3u Gemini C18 column (150 mm x 2 mm, particle size 3 µM, pore size 110A°; Phenomenex) operated at 40°C with a flow rate of 200 µL/min using an Ultimate 3000 HPLC system. Peptides were loaded at 1% solvent B (2 min) and eluted with a gradient of 1 – 50% B in 10 min, 50 – 78% B in 2 min and 1 min at 78% B. Fractions were collected in 50-s intervals (starting after 1 min, ending at 21 min) in a concatenated manner such that every 9th fraction was combined, which resulted in a total of 8 fractions per replicate. Peptides were dried in vacuo, desalted using StageTips as described before [135], and acidified by adding trifluoroacetic acid to a final concentration of 0.1% (v/v).

LC-MS analysis

Peptides were analyzed by nano-HPLC-tandem mass spectrometry (MS/MS) using an UltiMate 3000 RSLCnano system (Thermo Fisher Scientific, Dreieich, Germany) connected to an Orbitrap Elite mass spectrometer (Thermo Fisher Scientific, Bremen, Germany). The RSLC system was equipped with C18 pre-columns (nanoEase M/Z Symmetry C18; 20 mm length, 0.18 mm inner diameter; Waters) for washing and preconcentration of the peptides at a flow rate of 10 µL/min and an analytical C18 reversed-phase nano LC column (nanoEase M/Z HSS C18 T3; 250 mm length, 75 mm inner diameter, 1.8 µm particle size, 100 Å packing density; Waters) for peptide separation (flowrate, of 300 nl/min). Peptides were eluted using a binary solvent system that consisted of 4% (v/v) dimethyl sulfoxide (DMSO)/0.1% (v/v) formic acid (FA) (solvent A) and 4% (v/v) DMSO/0.1% (v/v) FA/30% (v/v) ACN/48% (v/v) methanol (solvent B). Peptides equivalent to 1 µg of protein were loaded onto the pre-columns for 5 min using solvent A and eluted applying a gradient ranging from 1 – 7% solvent B in 5 min, 7 – 52% B in 145 min, 52% – 95% B in 85 min, and 5 min at 95% B.

Mass spectrometric data were acquired in data-dependent mode using the following parameters: mass range of m/z 370 – 1700 for MS precursor scans at a resolution of 120,000 (at m/z 400); maximum automatic gain control (AGC) of 106 ions; maximum injection time (IT) of 200 ms. A TOP20 method was applied for low-energy collision-induced dissociation of precursor ions with a normalized collision energy of 35%, an activation q of 0.25, and an activation time of 10 ms. The maximum AGC for MS/MS scans was set to 5 × 103 ions, the maximum IT to 150 ms, and the dynamic exclusion time to 45 sec.

MS data analysis

For protein identification and relative quantification, the MaxQuant software package (version 1.6.10.43) [138] with its integrated search engine Andromeda [139] was employed. MS/MS data were searched against the *S. cere-*

visiae reference proteome provided by UniProt (www.uniprot.org/proteomes/UP000002311; downloaded April 2021; 6,079 entries). The database search was carried out using trypsin and LysC as proteolytic enzymes, allowing a maximum of three missed cleavages, and applying mass tolerances of 4.5 ppm for precursor and 0.5 Da for fragment ions. Carbamidomethylation of cysteine residues was set as fixed modification, oxidation of methionine and acetylation of protein N-termini were considered as variable modifications, and DimethLys0/DimethNter0 and DimethLys6/DimethNter6 were selected as light and heavy labels, respectively. The options 'match between runs' and 'requantify' were enabled. 'Requantify' enables the calculation of protein abundance ratios in experiments that employ stable isotope labeling if only the labeled or unlabeled variant of a peptide is present. For example, this is the case for Pex3 peptides, which are absent in *pex3* cells. Using the 'requantify' option, the algorithm assigns a peptide intensity for the missing counterpart from the background signals in MS spectra at the expected m/z value. Protein identification was based on ≥ one unique peptide with a minimum length of seven amino acids. A false discovery rate of 0.01 was applied at both peptide and protein levels. For relative protein quantification, ≥ one ratio count (considering unique and razor peptides) was required.

For data analysis and visualization, MaxQuant results were processed using the Python-based analysis pipeline "autoprot" [140]. Only proteins quantified in at least two out of three replicates were considered for further analysis. Normalized protein abundance ratios calculated by MaxQuant were log2-transformed, followed by sequential imputation of missing values and cyclic-loess normalization [141]. To identify proteins with differences in protein abundance between WT and *pex3* cells, we used the 'linear models for microarray data' (limma) approach, a moderated two-sided t-test that adjusts a protein's variance in ratios between replicates towards the average ratio variance of the entire dataset [142, 143]. Information about proteins identified and quantified are provided in Tables S1a and S1c. Information about peroxisomal localization of proteins or association with peroxisomes, used to assess the effect of *PEX3* deletion on peroxisomal proteins and transcripts, is based on published data [15, 16, 39-42].

Transcriptomics analysis

Cells were harvested by flash cooling the culture flasks on wet ice for 5 min followed by centrifugation for 7 min at 6000 g at 4°C. The supernatants were decanted, and pellets were subjected to an additional 1 min centrifugation to remove residual supernatant. After removal of the supernatant, the pellets were solubilized in RNAlater® (Sigma, #R0901) according to the instructions of the manufacturer and incubated on wet ice for 5 min. The samples were spun down for 10 min at 6000 g at 4°C and the supernatants were removed. The samples were centrifuged for an additional 1 min at 6000 g to remove residual supernatant and the cell pellets were flash frozen in liquid nitrogen, stored at -80°C and shipped on dry ice for further analysis.

Transcriptomic analysis was performed by Eurofins as a service package named NGSelect RNA analysis (Eurofins Germany, #6WB2-RNAI01). 150 ng total mRNA was used. The mRNA was poly-A purified and fragmented, followed by random primed cDNA library synthesis, adapter ligation and adapter specific PCR amplification. Sequencing was performed using the Illumina BIO-IT platform, as paired end with 5 million read pairs (2 x 150 bp) per sample. For reference, the *Saccharomyces cerevisiae* S288c assembly from the Saccharomyces Genome Database R64-1-1 (INSDC Assembly GCA_000146045.2, Sep 2011) was used [144].

For data analysis, genes with less than 10 reads on average across the compared groups were removed. The abundance counts of each gene were then used to perform differential gene expression (DGE) analysis [145]. DGE was performed using the R/Bioconductor DESeq2 package [146]. Standard normalization and differential expression analysis steps were subjected to a single function in DESeq2m using the function DESeqDataSetFromMatrix. P-values were calculated using the Wald test implemented in the R/Bioconductor DESeq2 package.

Gene Ontology term enrichment analysis

GO term enrichment analyses of proteins and transcripts exhibiting a minimum fold-change of 1.5 (reduced/increased; p-value < 0.05) in *pex3* compared to WT cells were performed using the shinyGO application (version 0.77; http://bioinformatics.sdstate.edu/go/) [147] and all proteins and transcripts identified in our omics analysis as background. False discovery rate p-values were corrected for multiple testing using the Benjamini-Hochberg method implemented in the shinyGO analysis pipeline. GO terms with corrected p-values of < 0.05 were considered enriched. The results of the GO term enrichment analyses are provided in Table S2.

Fluorescence microscopy

Widefield fluorescence microscopy images of living cells were captured in a growth medium at room temperature. Images were obtained using an Axioscope A1 microscope (Carl Zeiss), with a 100 × 1.30 NA objective, MicroManager 1.4 software, and a digital camera (Coolsnap HQ2; Photometrics). GFP and mNeonGreen fluorescence was visualized using a 470/40 nm band-pass excitation filter, a 495 nm dichromatic mirror, and a 525/50 nm band-pass emission filter. mKate2 and mCherry fluorescence was visualized using a 587/25 nm band-pass excitation

filter, a 605 nm dichromatic mirror, and a 670/70 nm band-pass emission filter.

Airyscan images were captured with a confocal microscope (LSM800; CarlZeiss) equipped with a 32 channel gallium arsenide phosphide photomultiplier tube (GaAsP-PMT), Zen 2009 software (CarlZeiss), and a 63×1.40 NA objective (CarlZeiss). The GFP signal was visualized by excitation with a 488 nm laser, and mCherry was visualized with a 561 nm laser. Mitotracker was visualized with a 561 nm laser. To stain mitochondria MitoTracker™ Red CMXRos (#M7512) was used according to manufacturer's protocol. For quantitative co-localization analysis cells were fixed in 1% formaldehyde for 30 min on ice and incubated in 10 mM glycine in 100 mM PBS (pH 7.5) for 60 min on ice.

Image analysis was performed using ImageJ [148] and Fiji [149]. Quantitative co-localization analysis was performed using the Fiji plug-in JACoP [150]. Brightfield images have been adjusted to only show cell contours.

Immunoblotting

Total cell extracts were prepared from trichloroacetic acid (TCA) treated cells as described previously [151, 152]. Sodium dodecyl sulfate–polyacrylamide gel electrophoresis (SDS-PAGE) was performed as described previously [151, 153]. Equal volumes of samples were loaded per lane.

Semi-dry transfer of proteins from the polyacrylamide gel to a nitrocellulose membrane (Amersham Protran 0.2 NC, #10600001) was performed as described before [154]. Blots were decorated with anti-pyruvate carboxylase-1 (Pyc1) antibodies (1:10,000 dilution) [155], anti-Pot1 (1:10,000) [156], anti-Pex14 (1:5,000) [157], anti-Pex5 (1:10,000) [157], anti-Pex3 (1:5,000) [44], anti-Pex11 (1:1,000) [158], anti-Cta1 (1:20,000) [159], anti-Pcs60 (1:10,000) [160], anti-Atp18 (kind gift from Nikolaus Pfanner/Nils Wiedemann, University of Freiburg, Germany), anti-Porin (Invitrogen, #459500), anti-Pgk1 (Invitrogen, #459250), or anti-HA (1:10,000 dilution) (Roche, #12CA5). Secondary goat anti-rabbit (Thermo Scientific, #31460), goat anti-mouse (Thermo Scientific, #31430), or rabbit anti-goat (Sigma-Aldrich, #A8919) antibodies conjugated to horseradish peroxidase (dilution of 1:5,000 each) were used for detection. Chemiluminescent (Amersham ECL Prime, #RPN2232; SuperSignalTM West Pico PLUS, Thermo Scientific, #34578; or SuperSignalTM West Femto, Thermo Scientific, #34096) detection was performed according to the manufacturers' guidelines (Bio-Rad, Chemidoc Imaging System). Blots were imaged and analyzed using the Bio-Rad ChemiDoc imaging System.

Immunoblot signals were quantified using Fiji/ImageJ (version 1.54k; [149]). Background signals were subtracted, signals for individual proteins were normalized to the respective loading control (either Porin or Pgk1), and the values determined for the WT cells were set to 1.0.

Quantitative real time PCR

Total RNA was isolated using the Promega ReliaPrepTM RNA isolation kit (# Z6010). Cells were resuspended in the kit's lysis buffer and disrupted using acid-washed beads in a cell homogenizer (Minilys). RNA (1 µg) was reverse transcribed into cDNA using the Transcriptor High Fidelity cDNA-Synthesis kit (Roche/Merck, #5081955001). The PowerUp SYBR Green Master Mix (ThermoFisher, #A25742) was used to perform quantitative real time PCR (qPCR). The relative mRNA expression levels of selected genes in WT, *pex3* and *pex3*+p*PEX3* cells (three biological replicates each) were determined using the 2(-Delta Delta CT) method; *ALG9* was used as internal reference. Data for each target were scaled to the respective WT levels for normalization and are expressed as mean ± standard error of the mean. The sequences of the primers used for the qPCR experiments are provided in Table S5.

Data Availability Statement

The mass spectrometry proteomics data have been deposited to the ProteomeXchange Consortium [161] via the PRIDE [162] partner repository and are accessible using the dataset identifier PXD047234. The remaining data are available on request.

AUTHOR CONTRIBUTION

IvdK and BW conceived the project and supervised the study. TK, HD, AKR, MPP, and MA performed the experiments. TK, AKR and MPP grew and harvested the cells. HD, SO performed proteomics and quantitative MS data analysis. Analysis of the transcriptomics data was performed by MA and HD. HD, SO and MA performed bioinformatics and statistical analysis. TK performed the acetate measurements and yeast growth analysis. TK and AKR constructed yeast strains, performed fluorescence microscopy and spot assays. MPP, TK, and AKR performed Western blot analyses. HD conducted qPCR experiments. TK, IvdK and BW wrote the original draft of the manuscript. TK, MPP, HD and SO prepared figures and tables. All authors contributed to reviewing and editing the manuscript. All authors approved the final version of the manuscript.

ACKNOWLEDGEMENTS

We thank Maya Schuldiner and Einat Zalckvar (Weizmann Institute) for making yeast strains available, Ralf Erdmann (Ruhr University Bochum) and Nils Wiedemann (University of Freiburg) for antibodies. We are grateful to Jeroen Nijland for performing the acetate measurements, to Rinse de Boer for assistance in preparing the microscopy images, and to Sven Spielhaupter for support in qPCR experiments. We thank Arjen Krikken, Rinse de Boer and Jan Kiel (RUG) for helpful discussions and expert technical assis-

tance. This project received funding from the European Union's Horizon 2020 research and innovation programme under the Marie Skłodowska-Curie grant agreement No 812968. Work included in this study has been performed in partial fulfillment of the doctoral thesis of H.D. at the University of Würzburg.

SUPPLEMENTAL MATERIAL

All supplemental data for this article are available online at www.microbialcell.com.

CONFLICT OF INTEREST

The authors declare no conflict of interest.

Please cite this article as: Tjasa Kosir, Hirak Das, Marc Pilegaard Pedersen, Ann-Kathrin Richard, Marco Anteghini, Vitor Martins dos Santos, Silke Oeljeklaus, Ida J. van der Klei and Bettina Warscheid (2025). Integrative Omics reveals changes in the cellular landscape of peroxisome-deficient *pex3* yeast cells. **Microbial Cell** 12: 9-33. doi: 10.15698/mic2025.02.842.

REFERENCES

1. Waterham HR, Ferdinandusse S, and Wanders RJA (**2016**). Human disorders of peroxisome metabolism and biogenesis. **Biochim Biophys Acta Mol Cell Res** 1863(5): 922–933. doi: 10.1016/j.bbamcr.2015.11.015

2. Bartoszewska M, Opaliński Ł, Veenhuis M, and van der Klei IJ (**2011**). The significance of peroxisomes in secondary metabolite biosynthesis in filamentous fungi. **Biotechnol Lett** 33(10): 1921–1931. doi: 10.1007/s10529-011-0664-y

3. Wanders RJA, and Waterham HR (**2006**). Biochemistry of mammalian peroxisomes revisited. **Annu Rev Biochem** 75(1): 295–332. doi: 10.1146/annurev.biochem.74.082803.133329

4. Hu J, Baker A, Bartel B, Linka N, Mullen RT, Reumann S, and Zolman BK (**2012**). Plant peroxisomes: Biogenesis and function. **Plant Cell** 24(6): 2279–2303. doi: 10.1105/tpc.112.096586

5. Wanders RJA, Baes M, Ribeiro D, Ferdinandusse S, and Waterham HR (**2023**). The physiological functions of human peroxisomes. **Physiol Rev** 103(1): 957–1024. doi: 10.1152/physrev.00051.2021

6. Jansen RLM, Santana-Molina C, van den Noort M, Devos DP, and van der Klei IJ (**2021**). Comparative genomics of peroxisome biogenesis proteins: Making sense of the PEX proteins. **Front Cell Dev Biol** 9: 654163. doi: 10.3389/fcell.2021.654163

7. Kumar R, Islinger M, Worthy H, Carmichael R, and Schrader M (**2024**). The peroxisome: an update on mysteries 3.0. **Histochem Cell Biol** 161(2): 99–132. doi: 10.1007/s00418-023-02259-5

8. Chornyi S, IJlst L, van Roermund CWT, Wanders RJA, and Waterham HR (**2021**). Peroxisomal Metabolite and Cofactor Transport in Humans. **Front Cell Dev Biol** 8: 613892. doi: 10.3389/fcell.2020.613892

9. Islinger M, Voelkl A, Fahimi HD, and Schrader M (**2018**). The peroxisome: an update on mysteries 2.0. **Histochem Cell Biol** 150(5): 443–471. doi: 10.1007/s00418-018-1722-5

10. Fransen M, Nordgren M, Wang B, Apanasets O, and Van Veldhoven PP (**2013**). Aging, age-related diseases and peroxisomes. In: del Rio LA, editor Peroxisomes and their Key Role in Cellular Signaling and Metabolism. **Springer**, pp 45–65.

11. Ferreira V, Ferreira AR, and Ribeiro D (**2023**). Peroxisomes and viruses: Overview on current knowledge and experimental approaches. In: Schrader M, editor Peroxisomes: Methods and Protocols. **Humana Press Inc.**; pp 271–294.

12. Erdmann R, Veenhuis M, and Kunau W-H (**1997**). Peroxisomes: Organelles at the crossroads. **Trends Cell Biol** 7(10): 400–407. doi: 10.1016/S0962-8924(97)01126-4

13. Akşit A, and van der Klei IJ (**2018**). Yeast peroxisomes: How are they formed and how do they grow? **Int J Biochem Cell Biol** 105: 24–34. doi: 10.1016/j.biocel.2018.09.019

14. Mast FD, and Aitchison JD (**2018**). Characterization of peroxisomal regulation networks. In: Schrader M, Luis A. del Río LA, editors Proteomics of Peroxisomes: Identifying Novel Functions and Regulatory Networks. **Springer**, pp 367–382.

15. Yifrach E, Holbrook-Smith D, Bürgi J, Othman A, Eisenstein M, van Roermund CW, Visser W, Tirosh A, Rudowitz M, Bibi C, Galor S, Weill U, Fadel A, Peleg Y, Erdmann R, Waterham HR, Wanders RJA, Wilmanns M, Zamboni N, Schuldiner M, and Zalckvar E (**2022**). Systematic multi-level analysis of an organelle proteome reveals new peroxisomal functions. **Mol Syst Biol** 18(9): e11186. doi: 10.15252/msb.202211186

16. Marelli M, Smith JJ, Jung S, Yi E, Nesvizhskii AI, Christmas RH, Saleem RA, Tam YYC, Fagarasanu A, Goodlett DR, Aebersold R, Rachubinski RA, and Aitchison JD (**2004**). Quantitative mass spectrometry reveals a role for the GTPase Rho1p in actin organization on the peroxisome membrane. **J Cell Biol** 167(6): 1099–1112. doi: 10.1083/jcb.200404119

17. David C, Koch J, Oeljeklaus S, Laernsack A, Melchior S, Wiese S, Schummer A, Erdmann R, Warscheid B, and Brocard C (**2013**). A combined approach of quantitative interaction proteomics and live-cell imaging reveals a regulatory role for endoplasmic reticulum (ER) reticulon homology proteins in peroxisome biogenesis. **Mol Cell Proteomics** 12(9): 2408–2425. doi: 10.1074/mcp.M112.017830

18. Mast FD, Jamakhandi A, Saleem RA, Dilworth DJ, Rogers RS, Rachubinski RA, and Aitchison JD (**2016**). Peroxins Pex30 and Pex29 dynamically associate with reticulons to regulate peroxisome biogenesis from the endoplasmic reticulum. **J Biol Chem** 291(30): 15408–15427. doi: 10.1074/jbc.M116.728154

19. Grunau S, Schliebs W, Linnepe R, Neufeld C, Cizmowski C, Reinartz B, Meyer HE, Warscheid B, Girzalsky W, and Erdmann R (**2009**). Peroxisomal targeting of PTS2 pre-import complexes in the yeast *Saccharomyces cerevisiae*. **Traffic** 10(4): 451–460. doi: 10.1111/j.1600-0854.2008.00876.x

20. Silva BSC, DiGiovanni L, Kumar R, Carmichael RE, Kim PK, and Schrader M (**2020**). Maintaining social contacts: The physiological relevance of organelle interactions. **Biochim Biophys Acta Mol Cell Res** 1867(11): 118800. doi: 10.1016/j.bbamcr.2020.118800

21. Shai N, Yifrach E, van Roermund CWT, Cohen N, Bibi C, IJlst L, Cavellini L, Meurisse J, Schuster R, Zada L, Mari MC, Reggiori FM, Hughes AL, Escobar-Henriques M, Cohen MM, Waterham HR, Wanders RJA, Schuldiner M, and Zalckvar E (**2018**). Systematic mapping of contact sites reveals tethers and a function for the peroxisome-mitochondria contact. **Nat Commun** 9(1): 1761. doi: 10.1038/s41467-018-03957-8

22. Enkler L, Szentgyörgyi V, Pennauer M, Prescianotto-Baschong C, Riezman I, Wiesyk A, Avraham RE, Spiess M, Zalckvar E, Kucharczyk R, Riezman H, and Spang A (**2023**). Arf1 coordinates fatty acid metabolism and mitochondrial homeostasis. **Nat Cell Biol** 25(8): 1157–1172. doi: 10.1038/s41556-023-01180-2

23. Wu F, de Boer R, and van der Klei IJ (**2023**). Gluing yeast peroxisomes – composition and function of membrane contact sites. **J Cell Sci** 136(11): jcs259440. doi: 10.1242/jcs.259440

24. Hettema EH, Girzalsky W, van den Berg M, Erdmann R, and Distel B (**2000**). *Saccharomyces cerevisiae* Pex3p and Pex19p are required for proper localization and stability of peroxisomal membrane proteins. **EMBO J** 19(2): 223–233. doi: 10.1093/emboj/19.2.223

25. Höhfeld J, Veenhuis M, and Kunau WH (**1991**). PAS3, a Saccharomyces cerevisiae gene encoding a peroxisomal integral membrane protein essential for peroxisome biogenesis. **J Cell Biol** 114(6): 1167–1178. doi: 10.1083/jcb.114.6.1167

26. Rudowitz M, and Erdmann R (**2023**). Import and quality control of peroxisomal proteins. **J Cell Sci** 136(15). doi: 10.1242/jcs.260999

27. Wróblewska JP, Cruz-Zaragoza LD, Yuan W, Schummer A, Chuartzman SG, de Boer R, Oeljeklaus S, Schuldiner M, Zalckvar E, Warscheid B, Erdmann R, and van der Klei IJ (**2017**). *Saccharomyces cerevisiae* cells lacking Pex3 contain membrane vesicles that harbor a subset of peroxisomal membrane proteins. **Biochim Biophys Acta Mol Cell Res** 1864(10): 1656–1667. doi: 10.1016/j.bbamcr.2017.05.021

28. Kunze M, Pracharoenwattana I, Smith SM, and Hartig A (**2006**). A central role for the peroxisomal membrane in glyoxylate cycle function. **Biochim Biophys Acta Mol Cell Res** 1763(12): 1441–1452. doi: 10.1016/j.bbamcr.2006.09.009

29. Breidenbach RW, and Beevers H (**1967**). Association of the glyoxylate cycle enzymes in a novel subcellular particle from castor bean endosperm. **Biochem Biophys Res Commun** 27(4): 462–469. doi: 10.1016/S0006-291X(67)80007-X

30. Kunze M, and Hartig A (**2013**). Permeability of the peroxisomal membrane: lessons from the glyoxylate cycle. **Front Physiol** 4: 204. doi: 10.3389/fphys.2013.00204

31. Lee YJ, Jang JW, Kim KJ, and Maeng PJ (**2011**). TCA cycle-independent acetate metabolism via the glyoxylate cycle in *Saccharomyces cerevisiae*. **Yeast** 28(2): 153–166. doi: 10.1002/yea.1828

32. Kayikci Ö, and Nielsen J (**2015**). Glucose repression in *Saccharomyces cerevisiae*. **FEMS Yeast Res** 15(6): fov068. doi: 10.1093/femsyr/fov068

33. Rosenthal M, Metzl-Raz E, Bürgi J, Yifrach E, Drwesh L, Fadel A, Peleg Y, Rapaport D, Wilmanns M, Barkai N, Schuldiner M, and Zalckvar E (**2020**). Uncovering targeting priority to yeast peroxisomes using an in-cell competition assay. **Proc Natl Acad Sci U S A** 117(35): 21432–21440. doi: 10.1073/pnas.1920078117

34. Yifrach E, Chuartzman SG, Dahan N, Maskit S, Zada L, Weill U, Yofe I, Olender T, Schuldiner M, and Zalckvar E (**2016**). Characterization of proteome dynamics in oleate reveals a novel peroxisome targeting receptor. **J Cell Sci** 129(21): 4067-4075. doi: 10.1242/jcs.195255

35. Nakatsukasa K, Nishimura T, Byrne SD, Okamoto M, Takahashi-Nakaguchi A, Chibana H, Okumura F, and Kamura T (**2015**). The ubiquitin ligase SCFUcc1 acts as a metabolic switch for the glyoxylate cycle. **Mol Cell** 59(1): 22–34. doi: 10.1016/j.molcel.2015.04.013

36. Schummer A, Maier R, Gabay-Maskit S, Hansen T, Mühlhäuser WWD, Suppanz I, Fadel A, Schuldiner M, Girzalsky W, Oeljeklaus S, Zalckvar E, Erdmann R, and Warscheid B (**2020**). Pex14p phosphorylation modulates import of citrate synthase 2 into peroxisomes in *Saccharomyces cerevisiae*. **Front Cell Dev Biol** 8: 549451. doi: 10.3389/fcell.2020.549451

37. Elgersma Y, van Roermund CW, Wanders RJ, and Tabak HF (**1995**). Peroxisomal and mitochondrial carnitine acetyltransferases of *Saccharomyces cerevisiae* are encoded by a single gene. **EMBO J** 14(14): 3472–3479. doi: 10.1002/j.1460-2075.1995.tb07353.x

38. van Roermund CWT (**1999**). Molecular characterization of carnitine-dependent transport of acetyl-CoA from peroxisomes to mitochondria in *Saccharomyces cerevisiae* and identification of a plasma membrane carnitine transporter, Agp2p. **EMBO J** 18(21): 5843–5852. doi: 10.1093/emboj/18.21.5843

39. Motley AM, Nuttall JM, and Hettema EH (**2012**). Pex3-anchored Atg36 tags peroxisomes for degradation in *Saccharomyces cerevisiae*. **EMBO J** 31(13): 2852–2868. doi: 10.1038/emboj.2012.151

40. David Y, Castro IG, Yifrach E, Bibi C, Katawi E, Yahav Har-Shai D, Brodsky S, Barkai N, Ravid T, Eisenstein M, Pietrokovski S, Schuldiner M, and Zalckvar E (**2022**). Pls1 Is a peroxisomal matrix protein with a role in regulating lysine biosynthesis. **Cells** 11(9): 1426. doi: 10.3390/cells11091426

41. Elbaz-Alon Y, Morgan B, Clancy A, Amoako TNE, Zalckvar E, Dick TP, Schwappach B, and Schuldiner M (**2014**). The yeast oligopeptide transporter Opt2 is localized to peroxisomes and affects glutathione redox homeostasis. **FEMS Yeast Res** 14(7): 1055-67. doi: 10.1111/1567-1364.12196

42. Tanaka C, Tan L-J, Mochida K, Kirisako H, Koizumi M, Asai E, Sakoh-Nakatogawa M, Ohsumi Y, and Nakatogawa H (**2014**). Hrr25 triggers selective autophagy–related pathways by phosphorylating receptor proteins. **J Cell Biol** 207(1): 91–105. doi: 10.1083/jcb.201402128

43. Boersema PJ, Raijmakers R, Lemeer S, Mohammed S, and Heck AJR (**2009**). Multiplex peptide stable isotope dimethyl labeling for quantitative proteomics. **Nat Protoc** 4(4): 484–494. doi: 10.1038/nprot.2009.21

44. Höhfeld J, Veenhuis M, and Kunau WH (**1991**). PAS3, a *Saccharomyces cerevisiae* gene encoding a peroxisomal integral membrane protein essential for peroxisome biogenesis. **J Cell Biol** 114(6): 1167–1178. doi: 10.1083/jcb.114.6.1167

45. Rehling P, Skaletz-Rorowski A, Girzalsky W, Voorn-Brouwer T, Franse MM, Distel B, Veenhuis M, Kunau W-H, and Erdmann R (**2000**). Pex8p, an intraperoxisomal peroxin of *Saccharomyces cerevisiae* required for protein transport into peroxisomes binds the PTS1 receptor Pex5p. **J Biol Chem** 275(5): 3593–3602. doi: 10.1074/jbc.275.5.3593

46. Platta HW, Grunau S, Rosenkranz K, Girzalsky W, and Erdmann R (**2005**). Functional role of the AAA peroxins in dislocation of the cycling PTS1 receptor back to the cytosol. **Nat Cell Biol** 7(8): 817–822. doi: 10.1038/ncb1281

47. Saffian D, Grimm I, Girzalsky W, and Erdmann R (**2012**). ATP-dependent assembly of the heteromeric Pex1p–Pex6p-complex of the peroxisomal matrix protein import machinery. **J Struct Biol** 179(2): 126–132. doi: 10.1016/j.jsb.2012.06.002

48. Ali AM, Atmaj J, Adawy A, Lunev S, Van Oosterwijk N, Yan SR, Williams C, and Groves MR (**2018**). The Pex4p–Pex22p complex from *Hansenula polymorpha*: biophysical analysis, crystallization and X-ray diffraction characterization. **Acta Crystallogr F Struct Biol Commun** 74(2): 76–81. doi: 10.1107/S2053230X17018428

49. Williams C, van den Berg M, Panjikar S, Stanley WA, Distel B, and Wilmanns M (**2012**). Insights into ubiquitin-conjugating enzyme/ co-activator interactions from the structure of the Pex4p:Pex22p complex. **EMBO J** 31(2): 391–402. doi: 10.1038/emboj.2011.411

50. Hiltunen JK, Mursula AM, Rottensteiner H, Wierenga RK, Kastaniotis AJ, and Gurvitz A (**2003**). The biochemistry of peroxisomal β-oxidation in the yeast *Saccharomyces cerevisiae*. **FEMS Microbiol Rev** 27(1): 35–64. doi: 10.1016/S0168-6445(03)00017-2

51. Gurvitz A, Mursula AM, Firzinger A, Hamilton B, Kilpeläinen SH, Hartig A, Ruis H, Hiltunen JK, and Rottensteiner H (**1998**). Peroxisomal Δ3-cis-Δ2-

trans-Enoyl-CoA Isomerase Encoded by ECI1 Is Required for Growth of the Yeast Saccharomyces cerevisiae on Unsaturated Fatty Acids. **J Biol Chem** 273(47): 31366–31374. doi: 10.1074/jbc.273.47.31366

52. Yang X, Edward Purdue P, and Lazarow PB (**2001**). Eci1p uses a PTS1 to enter peroxisomes: either its own or that of a partner, Dci1p. **Eur J Cell Biol** 80(2): 126–138. doi: 10.1078/0171-9335-00144

53. Gurvitz A, Mursula AM, Yagi AI, Hartig A, Ruis H, Rottensteiner H, and Hiltunen JK (**1999**). Alternatives to the isomerase-dependent pathway for the β-oxidation of oleic acid are dispensable in *Saccharomyces cerevisiae*. **J Biol Chem** 274(35): 24514–24521. doi: 10.1074/jbc.274.35.24514

54. Choudhry SK, Singh R, Williams CP, and van der Klei IJ (**2016**). Stress exposure results in increased peroxisomal levels of yeast Pnc1 and Gpd1, which are imported via a piggy-backing mechanism. **Biochim Biophys Acta Mol Cell Res** 1863(1): 148–156. doi: 10.1016/j.bbamcr.2015.10.017

55. Effelsberg D, Cruz-Zaragoza LD, Tonillo J, Schliebs W, and Erdmann R (**2015**). Role of Pex21p for piggyback import of Gpd1p and Pnc1p into Peroxisomes of *Saccharomyces cerevisiae*. **J Biol Chem** 290(42): 25333–25342. doi: 10.1074/jbc.M115.653451

56. van Roermund CWT, Drissen R, van den Berg M, Ijlst L, Hettema EH, Tabak HF, Waterham HR, and Wanders RJA (**2001**). Identification of a Peroxisomal ATP Carrier Required for Medium-Chain Fatty Acid β-Oxidation and Normal Peroxisome Proliferation in *Saccharomyces cerevisiae*. **Mol Cell Biol** 21(13): 4321–4329. doi: 10.1128/MCB.21.13.4321-4329.2001

57. Palmieri L, Rottensteiner H, Girzalsky W, Scarcia P, Palmieri F, and Erdmann R (**2001**). Identification and functional reconstitution of the yeast peroxisomal adenine nucleotide transporter. **EMBO J** 20(18): 5049–5059. doi: 10.1093/emboj/20.18.5049

58. Morgenstern M, Stiller SB, Lübbert P, Peikert CD, Dannenmaier S, Drepper F, Weill U, Höß P, Feuerstein R, Gebert M, Bohnert M, van der Laan M, Schuldiner M, Schütze C, Oeljeklaus S, Pfanner N, Wiedemann N, and Warscheid B (**2017**). Definition of a high-confidence mitochondrial proteome at quantitative scale. **Cell Rep** 19(13): 2836–2852. doi: 10.1016/j.celrep.2017.06.014

59. Bricker DK, Taylor EB, Schell JC, Orsak T, Boutron A, Chen Y-C, Cox JE, Cardon CM, Van Vranken JG, Dephoure N, Redin C, Boudina S, Gygi SP, Brivet M, Thummel CS, and Rutter J (**2012**). A mitochondrial pyruvate carrier required for pyruvate uptake in yeast, *Drosophila*, and humans. **Science** 337(6090): 96–100. doi: 10.1126/science.1218099

60. Tavoulari S, Thangaratnarajah C, Mavridou V, Harbour ME, Martinou J, and Kunji ER (**2019**). The yeast mitochondrial pyruvate carrier is a hetero-dimer in its functional state. **EMBO J** 38(10): e100785. doi: 10.15252/embj.2018100785

61. Bender T, Pena G, and Martinou J (**2015**). Regulation of mitochondrial pyruvate uptake by alternative pyruvate carrier complexes. **EMBO J** 34(7): 911–924. doi: 10.15252/embj.201490197

62. Herzig S, Raemy E, Montessuit S, Veuthey J-L, Zamboni N, Westermann B, Kunji ERS, and Martinou J-C (**2012**). Identification and functional expression of the mitochondrial pyruvate carrier. **Science** 337(6090): 93–96. doi: 10.1126/science.1218530

63. Albertsen M, Bellahn I, Krämer R, and Waffenschmidt S (**2003**). Localization and function of the yeast multidrug transporter Tpo1p. **J Biol Chem** 278(15): 12820–12825. doi: 10.1074/jbc.M210715200

64. do Valle Matta MA, Jonniaux J-L, Balzi E, Goffeau A, and van den Hazel B (**2001**). Novel target genes of the yeast regulator Pdr1p: a contribution of the TPO1 gene in resistance to quinidine and other drugs. **Gene** 272(1–2): 111–119. doi: 10.1016/S0378-1119(01)00558-3

65. Tomitori H, Kashiwangi K, Asakawa T, Kakinuma Y, Michael AJ, and Igarashi K (**2001**). Multiple polyamine transport systems on the vacuolar membrane in yeast. **Biochem J** 353(3): 681. doi: 10.1042/0264-6021:3530681

66. Tomitori H, Kashiwagi K, Sakata K, Kakinuma Y, and Igarashi K (**1999**). Identification of a gene for a polyamine transport protein in yeast. **J Biol Chem**.274(6): 3265–3267. doi: 10.1074/jbc.274.6.3265

67. Zhang X, Nijland JG, and Driessen AJM (**2022**). Combined roles of exporters in acetic acid tolerance in *Saccharomyces cerevisiae*. **Biotechnol Biofuels Bioprod** 15(1): 67. doi: 10.1186/s13068-022-02164-4

68. Hu Y, Zhu Z, Gradischnig D, Winkler M, Nielsen J, and Siewers V (**2020**). Engineering carboxylic acid reductase for selective synthesis of medium-chain fatty alcohols in yeast. **Proc Natl Acad Sci U S A** 117(37): 22974–22983. doi: 10.1073/pnas.2010521117

69. Nuebel E, Morgan JT, Fogarty S, Winter JM, Lettlova S, Berg JA, Chen Y, Kidwell CU, Maschek JA, Clowers KJ, Argyriou C, Chen L, Wittig I, Cox JE, Roh-Johnson M, Braverman N, Bonkowsky J, Gygi SP, and Rutter J (**2021**). The biochemical basis of mitochondrial dysfunction in Zellweger spectrum disorder. **EMBO Rep** 22(10). doi: 10.15252/embr.202051991

70. Breker M, Gymrek M, Moldavski O, and Schuldiner M (**2014**). LoQAtE—Localization and Quantitation ATlas of the yeast proteomE. A new tool for multiparametric dissection of single-protein behavior in response to biological perturbations in yeast. **Nucleic Acids Res** 42(D1): D726–D730. doi: 10.1093/nar/gkt933

71. Saerens SMG, Verstrepen KJ, Van Laere SDM, Voet ARD, Van Dijck P, Delvaux FR, and Thevelein JM (**2006**). The *Saccharomyces cerevisiae* EHT1 and EEB1 genes encode novel enzymes with medium-chain fatty acid ethyl ester synthesis and hydrolysis capacity. **J Biol Chem** 281(7): 4446–4456. doi: 10.1074/jbc.M512028200

72. Young ME, Karpova TS, Brügger B, Moschenross DM, Wang GK, Schneiter R, Wieland FT, and Cooper JA (**2002**). The Sur7p family defines novel cortical domains in *Saccharomyces cerevisiae*, affects sphingolipid metabolism, and is involved in sporulation. **Mol Cell Biol** 22(3): 927–934. doi: 10.1128/MCB.22.3.927-934.2002

73. Palavecino-Ruiz M, Bermudez-Moretti M, and Correa-Garcia S (**2017**). Unravelling the transcriptional regulation of *Saccharomyces cerevisiae* UGA genes: the dual role of transcription factor Leu3. **Microbiology** 163(11): 1692–1701. doi: 10.1099/mic.0.000560

74. Wu D, Xie W, Li X, Cai G, Lu J, and Xie G (**2020**). Metabolic engineering of *Saccharomyces cerevisiae* using the CRISPR/Cas9 system to minimize ethyl carbamate accumulation during Chinese rice wine fermentation. **Appl Microbiol Biotechnol** 104(10): 4435–4444. doi: 10.1007/s00253-020-10549-4

75. Coulon J, Husnik JI, Inglis DL, van der Merwe GK, Lonvaud A, Erasmus DJ, and van Vuuren HJJ (**2006**). Metabolic engineering of *Saccharomyces cerevisiae* to minimize the production of ethyl carbamate in wine. **Am J Enol Vitic** 57(2): 113–124. doi: 10.5344/ajev.2006.57.2.113

76. Chisholm G, and Cooper T (**1984**). *cis* -dominant mutations which dramatically enhance *DUR1,2* gene expression without affecting its normal regulation. **Mol Cell Biol** 4(5): 947–955. doi: 10.1128/mcb.4.5.947-955.1984

77. Schuberth C, Richly H, Rumpf S, and Buchberger A (**2004**). Shp1 and Ubx2 are adaptors of Cdc48 involved in ubiquitin-dependent protein degradation. **EMBO Rep** 5(8): 818–824. doi: 10.1038/sj.embor.7400203

78. Verma R, Oania R, Fang R, Smith GT, and Deshaies RJ (**2011**). Cdc48/p97 mediates UV-dependent turnover of RNA Pol II. **Mol Cell** 41(1): 82–92. doi: 10.1016/j.molcel.2010.12.017

79. Noireterre A, Serbyn N, Bagdiul I, and Stutz F (**2023**). Ubx5-Cdc48 assists the protease Wss1 at DNA-protein crosslink sites in yeast. **EMBO J** 42(13): e113609. doi: 10.15252/embj.2023113609

80. Li H, Ji Z, Paulo JA, Gygi SP, Rapoport TA, and Rapoport T (**2023**). Bidirectional substrate shuttling between the 26S proteasome and the Cdc48 ATPase promotes protein degradation. **bioRxiv**. doi: 10.1101/2023.12.20.572403

81. Estruch F, and Carlson M (**1990**). SNF6 encodes a nuclear protein that is required for expression of many genes in *Saccharomyces cerevisiae*. **Mol Cell Biol** 10(6): 2544–2553. doi: 10.1128/MCB.10.6.2544

82. Laurent BC, Treitel MA, and Carlson M (**1991**). Functional interdependence of the yeast SNF2, SNF5, and SNF6 proteins in transcriptional activation. **Proc Natl Acad Sci U S A** 88(7): 2687–2691. doi: 10.1073/pnas.88.7.2687

83. Cashikar AG, Duennwald M, and Lindquist SL (**2006**). A chaperone pathway in protein disaggregation: Hsp26 alters the nature of protein aggregates to facilitate reactivation by Hsp104. **J Biol Chem** 281(13): 8996. doi: 10.1016/S0021-9258(19)56607-8

84. Specht S, Miller SBM, Mogk A, and Bukau B (**2011**). Hsp42 is required for sequestration of protein aggregates into deposition sites in *Saccharomyces cerevisiae*. **J Cell Biol** 195(4): 617–629. doi: 10.1083/jcb.201106037

85. Krämer L, Dalheimer N, Räschle M, Storchová Z, Pielage J, Boos F, and Herrmann JM (**2023**). MitoStores: chaperone-controlled protein granules store mitochondrial precursors in the cytosol. **EMBO J** 42(7): e112309. doi: 10.15252/embj.2022112309

86. Bösl B, Grimminger V, and Walter S (**2006**). The molecular chaperone Hsp104—A molecular machine for protein disaggregation. **J Struct Biol** 156(1): 139–148. doi: 10.1016/j.jsb.2006.02.004

87. Welker S, Rudolph B, Frenzel E, Hagn F, Liebisch G, Schmitz G, Scheuring J, Kerth A, Blume A, Weinkauf S, Haslbeck M, Kessler H, and Buchner J (**2010**). Hsp12 is an intrinsically unstructured stress protein that folds upon membrane association and modulates membrane function. **Mol Cell** 39(4): 507–520. doi: 10.1016/j.molcel.2010.08.001

88. Sales K, Brandt W, Rumbak E, and Lindsey G (**2000**). The LEA-like protein HSP 12 in *Saccharomyces cerevisiae* has a plasma membrane location and protects membranes against desiccation and ethanol-induced stress. **Biochim Biophys Acta Biomembr** 1463(2): 267–278. doi: 10.1016/S0005-2736(99)00215-1

89. Tsai C, Aslam K, Drendel HM, Asiago JM, Goode KM, Paul LN, Rochet J-C, and Hazbun TR (**2015**). Hsp31 is a stress response chaperone that intervenes in the protein misfolding process. **J Biol Chem** 290(41): 24816–24834. doi: 10.1074/jbc.M115.678367

90. Voos W, and Röttgers K (**2002**). Molecular chaperones as essential mediators of mitochondrial biogenesis. **Biochim Biophys Acta Mol Cell Res** 1592(1): 51–62. doi: 10.1016/S0167-4889(02)00264-1

91. Baumann F, Milisav I, Neupert W, and Herrmann JM (**2000**). Ecm10, a novel Hsp70 homolog in the mitochondrial matrix of the yeast *Saccharomyces cerevisiae*. **FEBS Lett** 487(2): 307–312. doi: 10.1016/S0014-5793(00)02364-4

92. Pfanner N, Warscheid B, and Wiedemann N (**2019**). Mitochondrial proteins: from biogenesis to functional networks. **Nat Rev Mol Cell Biol** 20(5): 267–284. doi: 10.1038/s41580-018-0092-0

93. Kurita O (**1999**). Involvement of mitochondrial aldehyde dehydrogenase ALD5 in maintenance of the mitochondrial electron transport chain in *Saccharomyces cerevisiae*. **FEMS Microbiol Lett** 181(2): 281–287. doi: 10.1016/S0378-1097(99)00523-6

94. Saint-Prix F, Bönquist L, and Dequin S (**2004**). Functional analysis of the ALD gene family of *Saccharomyces cerevisiae* during anaerobic growth on glucose: the NADP+-dependent Ald6p and Ald5p isoforms play a major role in acetate formation. **Microbiology** 150(7): 2209–2220. doi: 10.1099/mic.0.26999-0

95. Venard R, Brèthes D, Giraud M-F, Vaillier J, Velours J, and Haraux F (**2003**). Investigation of the role and mechanism of IF1 and STF1 proteins, twin inhibitory peptides which interact with the yeast mitochondrial ATP synthase. **Biochemistry** 42(24): 7626–7636. doi: 10.1021/bi034394t

96. Das S, Mukherjee S, Bedi M, and Ghosh A (**2021**). Mutations in the yeast Cox12 subunit severely compromise the activity of the mitochondrial complex IV. **Biochemistry** 86(12–13): 1607–1623. doi: 10.1134/S0006297921120105

97. Rigby K, Zhang L, Cobine PA, George GN, and Winge DR (**2007**). Characterization of the cytochrome c oxidase assembly factor Cox19 of *Saccharomyces cerevisiae*. **J Biol Chem** 282(14): 10233–10242. doi: 10.1074/jbc.M610082200

98. Nobrega MP, Bandeira SCB, Beers J, and Tzagoloff A (**2002**). Characterization of COX19, a widely distributed gene required for expression of mitochondrial cytochrome oxidase. **J Biol Chem** 277(43): 40206–40211. doi: 10.1074/jbc.M207348200

99. Glerum DM, Shtanko A, and Tzagoloff A (**1996**). Characterization of COX17, a yeast gene involved in copper metabolism and assembly of cytochrome oxidase. **J Biol Chem** 271(24): 14504–14509. doi: 10.1074/jbc.271.24.14504

100. Dumont ME, Cardillo TS, Hayes MK, and Sherman F (**1991**). Role of cytochrome c heme lyase in mitochondrial import and accumulation of cytochrome c in *Saccharomyces cerevisiae*. **Mol Cell Biol** 11(11): 5487–5496. doi: 10.1128/MCB.11.11.5487

101. Möller-Hergt BV, Carlström A, Stephan K, Imhof A, and Ott M (**2018**). The ribosome receptors Mrx15 and Mba1 jointly organize cotranslational insertion and protein biogenesis in mitochondria. **Mol Biol Cell** 29(20): 2386–2396. doi: 10.1091/mbc.E18-04-0227

102. Truscott KN, Voos W, Frazier AE, Lind M, Li Y, Geissler A, Dudek J, Mu¨ller H, Sickmann A, Meyer HE, Meisinger C, Guiard B, Rehling P, and Pfanner N (**2003**). A J-protein is an essential subunit of the presequence translocase–associated protein import motor of mitochondria. **J Cell Biol** 163(4): 707–713. doi: 10.1083/jcb.200308004

103. Hansen KG, Aviram N, Laborenz J, Bibi C, Meyer M, Spang A, Schuldiner M, and Herrmann JM (**2018**). An ER surface retrieval pathway safeguards the import of mitochondrial membrane proteins in yeast. **Science** 361(6407): 1118–1122. doi: 10.1126/science.aar8174

104. Laborenz J, Bykov YS, Knöringer K, Räschle M, Filker S, Prescianotto-Baschong C, Spang A, Tatsuta T, Langer T, Storchová Z, Schuldiner M, and Herrmann JM (**2021**). The ER protein Ema19 facilitates the degradation of nonimported mitochondrial precursor proteins. **Mol Biol Cell** 32(8): 664–674. doi: 10.1091/mbc.E20-11-0748

105. Avci D, Fuchs S, Schrul B, Fukumori A, Breker M, Frumkin I, Chen C, Biniossek ML, Kremmer E, Schilling O, Steiner H, Schuldiner M, and Lemberg MK (**2014**). The yeast ER-intramembrane protease Ypf1 refines nutrient sensing by regulating transporter abundance. **Mol Cell** 56(5): 630–640. doi: 10.1016/j.molcel.2014.10.012

106. Erdmann R, Veenhuis M, Mertens D, and Kunau WH (**1989**). Isolation of peroxisome-deficient mutants of *Saccharomyces cerevisiae*. **Proc Natl Acad Sci U S A** 86(14): 5419–5423. doi: 10.1073/pnas.86.14.5419

107. Weill U, Yofe I, Sass E, Stynen B, Davidi D, Natarajan J, Ben-Menachem R, Avihou Z, Goldman O, Harpaz N, Chuartzman S, Kniazev K, Knoblach B, Laborenz J, Boos F, Kowarzyk J, Ben-Dor S, Zalckvar E, Herrmann JM, Rachubinski RA, Pines O, Rapaport D, Michnick SW, Levy ED, and Schuldiner M (**2018**). Genome-wide SWAp-Tag yeast libraries for proteome exploration. **Nat Methods** 15(8): 617–622. doi: 10.1038/s41592-018-0044-9

108. Breitling R, Sharif O, Hartman ML, and Krisans SK (**2002**). Loss of compartmentalization causes misregulation of ysine biosynthesis in pe-

roxisome-deficient yeast cells. **Eukaryot Cell** 1(6): 978–986. doi: 10.1128/EC.1.6.978-986.2002

109. Krshnan L, van de Weijer ML, and Carvalho P (**2022**). Endoplasmic reticulum–associated protein degradation. **Cold Spring Harb Perspect Biol** 14(12): a041247. doi: 10.1101/cshperspect.a041247

110. Ward CL, Omura S, and Kopito RR (**1995**). Degradation of CFTR by the ubiquitin-proteasome pathway. **Cell** 83(1): 121–127. doi: 10.1016/0092-8674(95)90240-6

111. Hiller MM, Finger A, Schweiger M, and Wolf DH (**1996**). ER Degradation of a Misfolded Luminal Protein by the Cytosolic Ubiquitin-Proteasome Pathway. **Science** 273(5282): 1725–1728. doi: 10.1126/SCIENCE.273.5282.1725

112. van Roermund CWT, IJlst L, Linka N, Wanders RJA, and Waterham HR (**2022**). Peroxisomal ATP uptake is provided by two adenine nucleotide transporters and the ABCD transporters. **Front Cell Dev Biol** 9: 788921. doi: 10.3389/fcell.2021.788921

113. Pedersen MP, Wolters JC, de Boer R, Krikken AM, and van der Klei IJ (**2023**). The *Hansenula polymorpha* mitochondrial carrier family protein Mir1 is dually localized at peroxisomes and mitochondria. **Biochim Biophys Acta Mol Cell Res** 1871(5): 119742. doi: 10.1016/j.bbamcr.2024.119742

114. Cepińska MN, Veenhuis M, van der Klei IJ, and Nagotu S (**2011**). Peroxisome fission is associated with reorganization of specific membrane proteins. **Traffic** 12(7): 925–937. doi: 10.1111/j.1600-0854.2011.01198.x

115. Karpichev I V., and Small GM (**1998**). Global regulatory functions of Oaf1p and Pip2p (Oaf2p), transcription factors that regulate genes encoding peroxisomal proteins in *Saccharomyces cerevisiae*. **Mol Cell Biol** 18(11): 6560–6570. doi: 10.1128/MCB.18.11.6560

116. Dmochowska A, Dignard D, Maleszka R, and Thomas DY (**1990**). Structure and transcriptional control of the *Saccharomyces cerevisiae* POX1 gene encoding acylcoenzyme A oxidase. **Gene** 88(2): 247–252. doi: 10.1016/0378-1119(90)90038-S

117. Baumgart E, Vanhorebeek I, Grabenbauer M, Borgers M, Declercq PE, Fahimi HD, and Baes M (**2001**). Mitochondrial alterations caused by defective peroxisomal biogenesis in a mouse model for Zellweger syndrome (PEX5 knockout mouse). **Am J Pathol** 159(4): 1477–1494. doi: 10.1016/S0002-9440(10)62534-5

118. Goldfischer S, Moore CL, Johnson AB, Spiro AJ, Valsamis MP, Wisniewski HK, Ritch RH, Norton WT, Rapin I, and Gartner LM (**1973**). Peroxisomal and mitochondrial defects in the cerebro-hepato-renal syndrome. **Science** 182(4107): 62–64. doi: 10.1126/science.182.4107.62

119. Antonenkov VD (**1989**). Dehydrogenases of the pentose phosphate pathway in rat liver peroxisomes. **Eur J Biochem** 183(1): 75–82. doi: 10.1111/j.1432-1033.1989.tb14898.x

120. Veenhuis M (**1992**). Peroxisome biogenesis and function in *Hansenula polymorpha*. **Cell Biochem Funct** 10(3): 175–184. doi: 10.1002/cbf.290100307

121. Tajima S (**2004**). Ureide biosynthesis in legume nodules. **Front Biosci** 9(1–3): 1374. doi: 10.2741/1345

122. Angermüller S, Islinger M, and Völkl A (**2009**). Peroxisomes and reactive oxygen species, a lasting challenge. **Histochem Cell Biol** 131(4): 459–463. doi: 10.1007/s00418-009-0563-7

123. Munck JM, Motley AM, Nuttall JM, and Hettema EH (**2009**). A dual function for Pex3p in peroxisome formation and inheritance. **J Cell Biol** 187(4): 463–471. doi: 10.1083/jcb.200906161

124. Lyschik S, Lauer AA, Roth T, Janitschke D, Hollander M, Will T, Hartmann T, Kopito RR, Helms V, Grimm MOW, and Schrul B (**2022**). PEX19 coordinates neutral lipid storage in cells in a peroxisome-independent fashion. **Front Cell Dev Biol** 10: 859052. doi: 10.3389/fcell.2022.859052

125. Schrul B, and Kopito RR (**2016**). Peroxin-dependent targeting of a lipid-droplet-destined membrane protein to ER subdomains. **Nat Cell Biol** 18(7): 740–751. doi: 10.1038/ncb3373

126. Zimmermann R, Lang S, Lerner M, Förster F, Nguyen D, Helms V, and Schrul B (**2021**). Quantitative Proteomics and Differential Protein Abundance Analysis after the Depletion of PEX3 from Human Cells Identifies Additional Aspects of Protein Targeting to the ER. **Int J Mol Sci** 22(23): 13028. doi: 10.3390/ijms222313028

127. Van Dijken LP, Otto R, and Harder W (**1976**). Growth of *Hansenula polymorpha* in a methanol-limited chemostat. **Arch Microbiol** 111(1–2): 137–144. doi: 10.1007/BF00446560

128. Yofe I, Weill U, Meurer M, Chuartzman S, Zalckvar E, Goldman O, Ben-Dor S, Schütze C, Wiedemann N, Knop M, Khmelinskii A, and Schuldiner M (**2016**). One library to make them all: streamlining the creation of yeast libraries via a SWAp-Tag strategy. **Nat Methods** 13(4): 371–378. doi: 10.1038/nmeth.3795

129. Meurer M, Duan Y, Sass E, Kats I, Herbst K, Buchmuller BC, Dederer V, Huber F, Kirrmaier D, Štefl M, Van Laer K, Dick TP, Lemberg MK, Khmelinskii A, Levy ED, and Knop M (**2018**). Genome-wide C-SWAT library for high-throughput yeast genome tagging. **Nat Methods** 15(8): 598–600. doi: 10.1038/s41592-018-0045-8

130. Huh W-K, Falvo J V., Gerke LC, Carroll AS, Howson RW, Weissman JS, and O'Shea EK (**2003**). Global analysis of protein localization in budding yeast. **Nature** 425(6959): 686–691. doi: 10.1038/nature02026

131. Knop M, Siegers K, Pereira G, Zachariae W, Winsor B, Nasmyth K, and Schiebel E (**1999**). Epitope tagging of yeast genes using a PCR-based strategy: more tags and improved practical routines. **Yeast** 15(10B): 963–972. doi: 10.1002/(SICI)1097-0061(199907)15:10B<963::AID-YEA399>3.0.CO;2-W

132. Faber KN, Haima P, Harder W, Veenhuis M, and AB G (**1994**). Highly-efficient electrotransformation of the yeast *Hansenula polymorpha*. **Curr Genet** 25(4): 305–310. doi: 10.1007/BF00351482

133. Smith PK, Krohn RI, Hermanson GT, Mallia AK, Gartner FH, Provenzano MD, Fujimoto EK, Goeke NM, Olson BJ, and Klenk DC (**1985**). Measurement of protein using bicinchoninic acid. **Anal Biochem** 150(1): 76–85. doi: 10.1016/0003-2697(85)90442-7

134. Dannenmaier S, Stiller SB, Morgenstern M, Lübbert P, Oeljeklaus S, Wiedemann N, and Warscheid B (**2018**). Complete native stable isotope labeling by amino acids of *Saccharomyces cerevisiae* for global proteomic analysis. **Anal Chem** 90(17): 10501–10509. doi: 10.1021/acs.analchem.8b02557

135. Peikert CD, Mani J, Morgenstern M, Käser S, Knapp B, Wenger C, Harsman A, Oeljeklaus S, Schneider A, and Warscheid B (**2017**). Charting organellar importomes by quantitative mass spectrometry. **Nat Commun** 8(1): 15272. doi: 10.1038/ncomms15272

136. Delmotte N, Lasaosa M, Tholey A, Heinzle E, and Huber CG (**2007**). Two-dimensional reversed-phase × ion-pair reversed-phase HPLC: An alternative approach to high-resolution peptide separation for shotgun proteome analysis. **J Proteome Res** 6(11): 4363–4373. doi: 10.1021/pr070424t

137. Morgenstern M, Peikert CD, Lübbert P, Suppanz I, Klemm C, Alka O, Steiert C, Naumenko N, Schendzielorz A, Melchionda L, Mühlhäuser WWD, Knapp B, Busch JD, Stiller SB, Dannenmaier S, Lindau C, Licheva M, Eickhorst C, Galbusera R, Zerbes RM, Ryan MT, Kraft C, Kozjak-Pavlovic V, Drepper F, Dennerlein S, Oeljeklaus S, Pfanner N, Wiedemann N, and Warscheid B (**2021**). Quantitative high-confidence human mitochondrial proteome and its dynamics in cellular context. **Cell Metab** 33(12): 2464-2483.e18. doi: 10.1016/j.cmet.2021.11.001

138. Cox J, and Mann M (**2008**). MaxQuant enables high peptide identification rates, individualized p.p.b.-range mass accuracies and proteome-wide protein quantification. **Nat Biotechnol** 26(12): 1367–1372. doi: 10.1038/nbt.1511

139. Cox J, Neuhauser N, Michalski A, Scheltema RA, Olsen J V., and Mann M (**2011**). Andromeda: A peptide search engine integrated into the MaxQuant environment. **J Proteome Res** 10(4): 1794–1805. doi: 10.1021/pr101065j

140. Bender J, Mühlhäuser WWD, Zimmerman JP, Drepper F, and Warscheid B (**2024**). Autoprot: Processing, analysis and visualization of proteomics data in Python. **bioRxiv**. doi: 10.1101/2024.01.18.571429

141. Cleveland WS, and Devlin SJ (**1988**). Locally weighted regression: An approach to regression analysis by local fitting. **J Am Stat Assoc** 83(403): 596–610. doi: 10.1080/01621459.1988.10478639

142. Smyth GK (**2004**). Linear models and empirical bayes methods for assessing differential expression in microarray experiments. **Stat Appl Genet Mol Biol**.3(1): 1–25. doi: 10.2202/1544-6115.1027

143. Schwämmle V, León IR, and Jensen ON (**2013**). Assessment and improvement of statistical tools for comparative proteomics analysis of sparse data sets with few experimental replicates. **J Proteome Res** 12(9): 3874–3883. doi: 10.1021/pr400045u

144. Liachko I, Youngblood RA, Keich U, and Dunham MJ (**2013**). High-resolution mapping, characterization, and optimization of autonomously replicating sequences in yeast. **Genome Res** 23(4): 698–704. doi: 10.1101/gr.144659.112

145. Oshlack A, Robinson MD, and Young MD (**2010**). From RNA-seq reads to differential expression results. **Genome Biol** 11(12): 220. doi: 10.1186/gb-2010-11-12-220

146. Love MI, Huber W, and Anders S (**2014**). Moderated estimation of fold change and dispersion for RNA-seq data with DESeq2. **Genome Biol** 15(12): 550. doi: 10.1186/s13059-014-0550-8

147. Ge SX, Jung D, and Yao R (**2020**). ShinyGO: a graphical gene-set enrichment tool for animals and plants. **Bioinformatics** 36(8): 2628–2629. doi: 10.1093/bioinformatics/btz931

148. Schneider CA, Rasband WS, and Eliceiri KW (**2012**). NIH Image to ImageJ: 25 years of image analysis. **Nat Methods** 9(7): 671–675. doi: 10.1038/nmeth.2089

149. Schindelin J, Arganda-Carreras I, Frise E, Kaynig V, Longair M, Pietzsch T, Preibisch S, Rueden C, Saalfeld S, Schmid B, Tinevez J-Y, White DJ, Hartenstein V, Eliceiri K, Tomancak P, and Cardona A (**2012**). Fiji: an open-source platform for biological-image analysis. **Nat Methods** 9(7): 676–682. doi: 10.1038/nmeth.2019

150. Bolte S, and Cordelières FP (**2006**). A guided tour into subcellular colocalization analysis in light microscopy. **J Microsc** 224(3): 213–232. doi: 10.1111/j.1365-2818.2006.01706.x

151. Baerends RJS, Faber KN, Kram AM, Kiel JAKW, van der Klei IJ, and Veenhuis M (**2000**). A stretch of positively charged amino acids at the N terminus of *Hansenula polymorpha* Pex3p is involved in incorporation of the protein into the peroxisomal membrane. **J Biol Chem** 275(14): 9986–9995. doi: 10.1074/jbc.275.14.9986

152. McCammon M, McNew J, Willy P, and Goodman J (**1994**). An internal region of the peroxisomal membrane protein PMP47 is essential for sorting to peroxisomes. **J Cell Biol** 124(6): 915–925. doi: 10.1083/jcb.124.6.915

153. Laemmli UK (**1970**). Cleavage of structural proteins during the assembly of the head of bacteriophage T4. **Nature** 227(5259): 680–685. doi: 10.1038/227680a0

154. Kyhse-Andersen J (**1984**). Electroblotting of multiple gels: a simple apparatus without buffer tank for rapid transfer of proteins from polycrylamide to nitrocellulose. **J Biochem Biophys Methods** 10(3–4): 203–209. doi: 10.1016/0165-022X(84)90040-X

155. Ozimek PZ, Klompmaker SH, Visser N, Veenhuis M, and van der Klei IJ (**2007**). The transcarboxylase domain of pyruvate carboxylase is essential for assembly of the peroxisomal flavoenzyme alcohol oxidase. **FEMS Yeast Res** 7(7): 1082–1092. doi: 10.1111/j.1567-1364.2007.00214.x

156. Erdmann R, and Kunau W (**1994**). Purification and immunolocalization of the peroxisomal 3-oxoacyl-coA thiolase from *Saccharomyces cerevisiae*. **Yeast** 10(9): 1173–1182. doi: 10.1002/yea.320100905

157. Albertini M, Rehling P, Erdmann R, Girzalsky W, Kiel JAKW, Veenhuis M, and Kunau W-H (**1997**). Pex14p, a peroxisomal membrane protein binding both receptors of the two PTS-dependent import pathways. **Cell** 89(1): 83–92. doi: 10.1016/S0092-8674(00)80185-3

158. Erdmann R, and Blobel G (**1995**). Giant peroxisomes in oleic acid-induced *Saccharomyces cerevisiae* lacking the peroxisomal membrane protein Pmp27p. **J Cell Biol** 128(4): 509–523. doi: 10.1083/jcb.128.4.509

159. Kragler F, Langeder A, Raupachova J, Binder M, and Hartig A (**1993**). Two independent peroxisomal targeting signals in catalase A of Saccharomyces cerevisiae. **J Cell Biol** 120(3): 665–673. doi: 10.1083/jcb.120.3.665

160. Blobel F, and Erdmann R (**1996**). Identification of a Yeast Peroxisomal Member of the Family of AMP-Binding Proteins. **Eur J Biochem** 240(2): 468–476. doi: 10.1111/j.1432-1033.1996.0468h.x

161. Deutsch EW, Bandeira N, Perez-Riverol Y, Sharma V, Carver JJ, Mendoza L, Kundu DJ, Wang S, Bandla C, Kamatchinathan S, Hewapathirana S, Pullman BS, Wertz J, Sun Z, Kawano S, Okuda S, Watanabe Y, MacLean B, MacCoss MJ, Zhu Y, Ishihama Y, and Vizcaíno JA (**2023**). The ProteomeXchange consortium at 10 years: 2023 update. **Nucleic Acids Res** 51(D1): D1539–D1548. doi: 10.1093/nar/gkac1040

162. Perez-Riverol Y, Bai J, Bandla C, García-Seisdedos D, Hewapathirana S, Kamatchinathan S, Kundu DJ, Prakash A, Frericks-Zipper A, Eisenacher M, Walzer M, Wang S, Brazma A, and Vizcaíno JA (**2022**). The PRIDE database resources in 2022: a hub for mass spectrometry-based proteomics evidences. **Nucleic Acids Res** 50(D1): D543–D552. doi: 10.1093/nar/gkab1038

163. Koch C, Schuldiner M, and Herrmann JM (**2021**). ER-SURF: Riding the Endoplasmic Reticulum Surface to Mitochondria. **Int J Mol Sci** 22(17): 9655. doi: 10.3390/ijms22179655

164. Saraya R, Krikken AM, Kiel JAKW, Baerends RJS, Veenhuis M, and Klei IJ (**2012**). Novel genetic tools for *Hansenula polymorpha*. **FEMS Yeast Res** 12(3): 271–278. doi: 10.1111/j.1567-1364.2011.00772.x

165. Krikken AM, Wu H, de Boer R, Devos DP, Levine TP, and van der Klei IJ (**2020**). Peroxisome retention involves Inp1-dependent peroxisome–plasma membrane contact sites in yeast. **J Cell Biol** 219(10): e201906023. doi: 10.1083/jcb.201906023

166. Thomas AS, Krikken AM, de Boer R, and Williams C (**2018**). *Hansenula polymorpha* Aat2p is targeted to peroxisomes via a novel Pex20p-dependent pathway. **FEBS Lett** 592(14): 2466–2475. doi: 10.1002/1873-3468.13168

167. Saraya R, Cepińska MN, Kiel JAKW, Veenhuis M, and der Klei IJ van (**2010**). A conserved function for Inp2 in peroxisome inheritance. **Biochim Biophys Acta Mol Cell Res** 1803(5): 617–622. doi: 10.1016/j.bbamcr.2010.02.001

168. Saraya R (**2010**). Peroxisome formation and dynamics in yeast. **University of Groningen**.